

SEARCH FOR POST-MERGER GRAVITATIONAL WAVES FROM THE REMNANT OF THE BINARY
NEUTRON STAR MERGER GW170817

THE LIGO SCIENTIFIC COLLABORATION AND THE VIRGO COLLABORATION

ABSTRACT

The first observation of a binary neutron star coalescence by the Advanced LIGO and Advanced Virgo gravitational-wave detectors offers an unprecedented opportunity to study matter under the most extreme conditions. After such a merger, a compact remnant is left over whose nature depends primarily on the masses of the inspiralling objects and on the equation of state of nuclear matter. This could be either a black hole or a neutron star (NS), with the latter being either long-lived or too massive for stability implying delayed collapse to a black hole. Here, we present a search for gravitational waves from the remnant of the binary neutron star merger GW170817 using data from Advanced LIGO and Advanced Virgo. We search for short ($\lesssim 1$ s) and intermediate-duration ($\lesssim 500$ s) signals, which includes gravitational-wave emission from a hypermassive NS or supramassive NS, respectively. We find no signal from the post-merger remnant, which is consistent with estimated search strain sensitivities still more than an order of magnitude below the signal strengths predicted from most theoretical models. For short signals, our best upper limit on the root-sum-square of the gravitational-wave strain emitted from 1–4 kHz is $h_{\text{rSS}}^{50\%} = 2.1 \times 10^{-22} \text{ Hz}^{-1/2}$ at 50% detection efficiency. For intermediate-duration signals, our best upper limit at 50% detection efficiency is $h_{\text{rSS}}^{50\%} = 8.4 \times 10^{-22} \text{ Hz}^{-1/2}$ for a millisecond magnetar model, and $h_{\text{rSS}}^{50\%} = 5.9 \times 10^{-22} \text{ Hz}^{-1/2}$ for a bar-mode model. These results indicate that post-merger emission from a similar event may be detectable when advanced detectors reach design sensitivity or with next-generation detectors.

1. INTRODUCTION

On August 17, 2017 12:41:04.4 UTC, the two detectors of the Advanced Laser Interferometer Gravitational-Wave Observatory (LIGO) and the Advanced Virgo detector observed GW170817, the gravitational wave (GW) signal from the coalescence of two compact objects, almost certainly neutron stars (NSs) (Abbott et al. 2017a). Supporting this hypothesis were electromagnetic counterparts observed across the spectrum (Abbott et al. 2017b,c). Thanks to its relatively close proximity to Earth, with 90% credible intervals of 40_{-14}^{+8} Mpc as measured by the GW data analysis (Abbott et al. 2017a) and $43.8_{-6.9}^{+2.9}$ Mpc as measured with electromagnetic observations (Abbott et al. 2017d), GW170817 offers the first opportunity to study the nature of the remnant leftover from a binary NS merger using GW observations.

The merger of two NSs can have four possible outcomes: (i) The prompt formation of a black hole (BH), (ii) the formation of a hypermassive NS that collapses to a BH in $\lesssim 1$ s, (iii) the formation of a supramassive NS that collapses to a BH on timescales of $\sim 10 - 10^4$ s, or (iv) the formation of a stable NS. The specific outcome of any merger depends on the progenitor masses, with the two NSs that merged in GW170817 having a total mass between 2.73 and 3.29 M_{\odot} (using the high-spin priors) (Abbott et al. 2017a), and also on the NS equation of state. We present a broad search for both short ($\lesssim 1$ s) and intermediate ($\lesssim 500$ s) duration GW signals potentially emitted from post-merger remnants in scenarios (ii), (iii) and (iv). We find no evidence for a statistically significant signal and set upper limits on possible GW strain amplitudes and GW energy emission.

Before describing the search, we briefly review the four scenarios listed above. If the system promptly forms a BH, the GW quasinormal-mode ringdown signal from a remnant BH in the GW170817 mass range has a dominant frequency around 6 kHz (Shibata & Taniguchi 2006; Baiotti et al. 2008). Current GW detectors are not robustly calibrated at such high frequencies. Moreover, for such a remnant BH the ringdown signal-to-noise ratio at ~ 40 Mpc is vanishingly small. We therefore focus on short and intermediate-duration GW signals from a possible NS remnant. We also do not target GW emission from a delayed NS-to-BH collapse in scenarios (ii) or (iii), as it would be many orders of magnitude weaker and unlikely to be detectable (e.g., Baiotti et al. 2007).

A hypermassive NS is one that has mass greater than the maximum mass of a uniformly rotating star, but is prevented from collapse through being supported by differential rotation and thermal gradients (Baumgarte

et al. 2000). Rapid cooling through neutrino emission and magnetic braking of the differential rotation causes such merger remnants to collapse $\lesssim 1$ s after formation (Shapiro 2000; Hotokezaka et al. 2013). If, however, the star is lighter but still supramassive—i.e., its mass is larger than the maximum for a non-rotating NS—it will spin down through electromagnetic and GW emission, eventually collapsing to a BH on an expected timescale of 10 to $\lesssim 5 \times 10^4$ s after merger (Ravi & Lasky 2014).

Taking the posterior distributions for the progenitor masses (Abbott et al. 2017a), one can calculate a probability distribution for the gravitational mass of the post-merger remnant assuming conservation of baryonic mass (and neglecting mass loss to the ejecta). For a broad range of equations of state, this post-merger mass lies in the hypermassive NS regime (see Sec. 5.2 of Abbott et al. 2017c).

Moreover, observations of a kilonova-like counterpart in the optical and infrared can give insight into the resulting object. For example, observations suggest low-lanthanide ejecta from the merger (Smartt et al. 2017), which may be the result of a hypermassive NS surviving $\gtrsim 100$ ms after the merger, causing additional neutrino flux over that of prompt BH formation to irradiate the ejecta, increasing the electron fraction and not allowing the formation of lanthanides (Metzger & Fernández 2014; Abbott et al. 2017c,e). However, optical observations at late times also support opacity-heavy models, potentially implying a hypermassive NS lifetime < 100 ms (Smartt et al. 2017).

A hypermassive NS remnant may also partially explain the delay between the coalescence time of GW170817 and the trigger time of the short γ -ray burst (GRB) 170817A, detected 1.7 s later by the *Fermi* Gamma-ray Burst Monitor (Goldstein et al. 2017; Abbott et al. 2017c).

Simulations of merging binary NSs with hypermassive remnants show that the post-merger GW emission is dominated by the quadrupolar f -mode ($\sim 2-4$ kHz; Xing et al. 1994; Ruffert et al. 1996; Shibata & Uryū 2000), with broad secondary and tertiary peaks in the $\sim 1.8-4$ kHz range (Hotokezaka et al. 2013). Depending on the equation of state (EOS), the GW signal may include contributions from post-merger emission beginning around 1 kHz (Maione et al. 2017). The structure and locations of the spectral peaks is correlated with the masses and spins of the progenitors (Bernuzzi et al. 2014; Kastaun & Galeazzi 2015; Bauswein & Stergioulas 2015) and the nuclear equation of state (Read et al. 2013; Bernuzzi et al. 2015a; Rezzolla & Takami 2016), implying GW observations of a hypermassive NS potentially

enable strong constraints on the equation of state (Shibata 2005; Bauswein & Janka 2012).

We also consider the scenarios (iii) and (iv) of a longer-lived post-merger remnant. Observations of X-ray afterglows following short GRBs indicate that a fraction of binary NS mergers may result in supramassive or stable NSs lasting $\gg 100$ s (e.g., Rowlinson et al. 2013; Lü et al. 2015). GRB 170817A was sub-energetic compared to the population of cosmological short GRBs (Berger 2014; Abbott et al. 2017b; Goldstein et al. 2017), had an atypical X-ray afterglow (Evans et al. 2017; Troja et al. 2017), and had no observations hinting at a central engine remaining active following the GRB emission phase. Nevertheless, no electromagnetic observations rule out a longer-lived post-merger remnant for GW170817.

Gravitational-wave emission mechanisms in this scenario include magnetic field-induced ellipticities (Bonazzola & Gourgoulhon 1996; Palomba 2001; Cutler 2002), unstable bar modes (Lai & Shapiro 1995; Corsi & Mészáros 2009), and unstable r -modes (Lindblom et al. 1998; Andersson 1998). Estimates for the GW amplitude and detectability from such events vary across many orders of magnitude (e.g., Corsi & Mészáros 2009; Fan et al. 2013; Dall’Osso et al. 2015; Doneva et al. 2015; Lasky & Glampedakis 2016, and Sec. 4).

In summary, electromagnetic observations of this system do not provide definitive evidence for or against any of the four possible post-merger outcomes, motivating this broad search using data-analysis algorithms which are robust to uncertain waveform morphologies. We do not find any candidate post-merger GW signals associated with GW170817. This is not surprising; even considering the stronger potential GW emission from the hypermassive or supramassive NS phases, the signal-to-noise ratio for a post-merger signal from ~ 40 Mpc in the current LIGO-Virgo network would be less than ~ 1 - 2 even for a matched-filter search (Takami et al. 2014; Clark et al. 2016). However, we find that our current GW amplitude sensitivity is within approximately one order of magnitude of theoretical models for post-merger GW emission, implying that, with algorithmic improvements and the LIGO-Virgo network operating at design sensitivity (Abbott et al. 2016a), as well as future detectors, such emission might become detectable.

This paper is organized as follows. In Sec. 2 we describe the detectors and data set used. In Sec. 3 we present the search methods and results for both short- and intermediate-duration GW signals. We discuss the implications and outlook for the future in Sec. 4.

2. DETECTORS AND DATA QUALITY

The LIGO (Aasi et al. 2015), Virgo (Acernese et al. 2015), and GEO600 (Dooley et al. 2016) detectors were operating at the time of GW170817. The noise amplitude spectral densities are shown in Fig. 1, where the general trend of the detectors’ sensitivities at high frequencies is due to the reduced interferometer response, interrupted by non-stationary spectral features, many of which have known origins. The noise spectrum of LIGO Hanford is higher than that from Livingston in the frequency band from 100 Hz to 1 kHz; one contribution is correlated laser noise that can be subtracted off-line (Driggers et al. 2017, used e.g. for the parameter estimation in Abbott et al. 2017a). This search did not make use of such noise subtraction methods. Virgo suffered from large noise fluctuations and non-stationary spectral features at frequencies above 2.5 kHz (Acernese et al. 2015).

Due to a lack of detailed data quality studies available about GEO600, similar to those performed for LIGO and Virgo, data from that detector was not used in this analysis, although the sensitivity to a signal with time and sky location consistent with GW170817 would be roughly equal in Virgo and GEO600. We note, however, that the network signal-to-noise ratio was dominated by the two LIGO detectors.

The algorithm used to search for short-duration signals (Coherent Wave Burst, *cWB*) used only LIGO data from 1024–4096 Hz. Two algorithms were used for intermediate-duration signals: The Stochastic Transient Analysis Multi-detector Pipeline (*STAMP*) searched from 24–2000 Hz and 2000–4000 Hz in LIGO-only data, while *cWB* searches from 24–2048 Hz and used LIGO-Virgo data. These algorithms are described in Sec. 3.

We whitened and removed stationary spectral lines of instrumental origin. Other techniques were employed to minimize the impact of non-stationary spectral features (Abbott et al. 2017f). The data quality of the detectors was checked using the methods applied to previous gravitational-wave detections (Abbott et al. 2016b). A short-duration instrumental disturbance occurred in the Livingston detector 1.1 s before the coalescence time. Although this transient does not affect the performance of *cWB*, the *STAMP* analysis uses data in which the glitch is subtracted from the data (see Fig. 2 in Abbott et al. 2017a).

LIGO’s calibration uncertainty is 7% in amplitude and 3 degrees in phase below 2 kHz (Abbott et al. 2017a), and 8% in amplitude and 4 degrees in phase above 2 kHz (Cahillane et al. 2017). Virgo’s calibration uncertainty is 10% in amplitude and 10 degrees in phase up to 5 kHz (Abbott et al. 2017a). Calibration uncertain-

ties are not taken into account in calculations of upper limits.

3. SEARCH METHODS AND DETECTION EFFICIENCIES

In situations with great theoretical uncertainties, where no complete set of accurate GW template waveforms is available, a matched-filter search is not feasible. Instead, an efficient solution is to search for excess power in spectrograms (also called frequency-time or ft -maps) of GW detector data (Anderson et al. 2000; Klimentko & Mitselmakher 2004). Pattern recognition algorithms are used to identify the presence of GW signals in these maps (Thrane & Coughlin 2013; Sutton et al. 2010; Thrane et al. 2011; Cornish & Littenberg 2015; Klimentko et al. 2016). Here, to account for the large uncertainty in the nature of the remnant, we employ a number of algorithms, each designed to coherently combine data from multiple GW detectors, with different data-processing and clustering techniques that make them respond differently to different waveform models. These algorithms are designed to be sensitive to a wide variety of signal morphologies, and while we test their sensitivity to a number of post-merger waveform models, they are designed so as to be robust against the significant theoretical uncertainties by using generic clustering schemes. Each algorithm performs the search at a single sky position, which we take to be the direction of the host galaxy for the optical counterpart, NGC4993 (RA = 13.1634 hrs, Dec. = -23.3815° ; Coulter et al. 2017; Abbott et al. 2017b). Below, we briefly describe each algorithm used in this search and present their findings.

3.1. Short duration ($\lesssim 1$ s) signals

We perform an analysis targeting short-duration, high-frequency GWs near the time of coalescence designed to be sensitive to unmodeled signals. This search for GW bursts is performed using the cWB algorithm (Klimentko et al. 2016). We search for statistically significant coherent excess power due to GW bursts in a 2 s long window which begins at 1187008882 GPS time, includes the estimated time of coalescence, and extends forward in time covering the entire delay between the merger and the GRB (1.7 s, Abbott et al. 2017c).

The cWB algorithm performs a maximum likelihood evaluation of coherent excess power in a multi-resolution Wilson-Daubechies-Meyer wavelet transform, which is performed on the strain from each detector (Klimentko et al. 2016). The analysis ranks candidate events by their coherent network signal-to-noise ratio. Statistical significance of candidate events is found by com-

paring the ranking statistic with a background distribution measured from 5.6 days of coincident data from Livingston and Hanford during the period 13–21 August. This data is “time-shifted,” which means that a non-physical time lag is introduced between the detector analyzed so as to remove correlated gravitational-wave signals. This data is also “off-source,” which means it is outside of the 2 s window over which gravitational waves are searched for. This analysis yields an estimate of the false-alarm probability for a given possible detection.

We search over a frequency range of 1024–4096 Hz. No significant events are found within the 2 s “on-source” window. The sensitivity of the cWB analysis is characterized through Monte-Carlo simulations in which waveforms from binary NS post-merger simulations are added to data from off-source periods (see Appendix A.1 for details). The simulated sources are placed at the known sky-location of the optical counterpart of GW170817 and with orbital inclination consistent with the pre-merger analysis (Abbott et al. 2017a). The waveform amplitudes are varied to determine the efficiency as a function of signal strength; see Abbott et al. (2017f) for an expanded discussion. The response of a given detector to the impinging GW is assumed to take the form

$$s(t) = F_+(\Theta, \psi)h_+(t) + F_\times(\Theta, \psi)h_\times(t), \quad (1)$$

where F_+ and F_\times are the antenna patterns for a given detector, Θ encodes the direction to the source and ψ is the polarization angle.

It is customary to express the sensitivity of a search to a given model waveform in $h_{\text{rSS}}^{50\%}$, which is the root-sum-squared strain amplitude of signals which are detected with 50% efficiency Abbott et al. (2017f). The detection criterion has been chosen in this specific search by setting a detection threshold on the significance of candidates which corresponds to a false-alarm probability of 10^{-4} . The quantity h_{rSS} is defined as

$$h_{\text{rSS}} = \sqrt{2 \int_{f_{\text{min}}}^{f_{\text{max}}} (|\tilde{h}_+(f)|^2 + |\tilde{h}_\times(f)|^2) df}, \quad (2)$$

where f_{min} and f_{max} are respectively the minimum and maximum frequencies over which the search is performed. The search sensitivities are shown in Fig. 1 and Table A.1 in terms of the average frequency of each waveform, \bar{f} . We also provide as a point of comparison the h_{rSS} of the same NR waveforms used in the analysis but assuming the distance of GW170817. It is worth noting that softer EOSs which lead to more compact stars exhibit a longer duration, higher frequency inspiral phase (Bauswein et al. 2013b) and a more dense remnant with relatively high frequency post-merger oscillations.

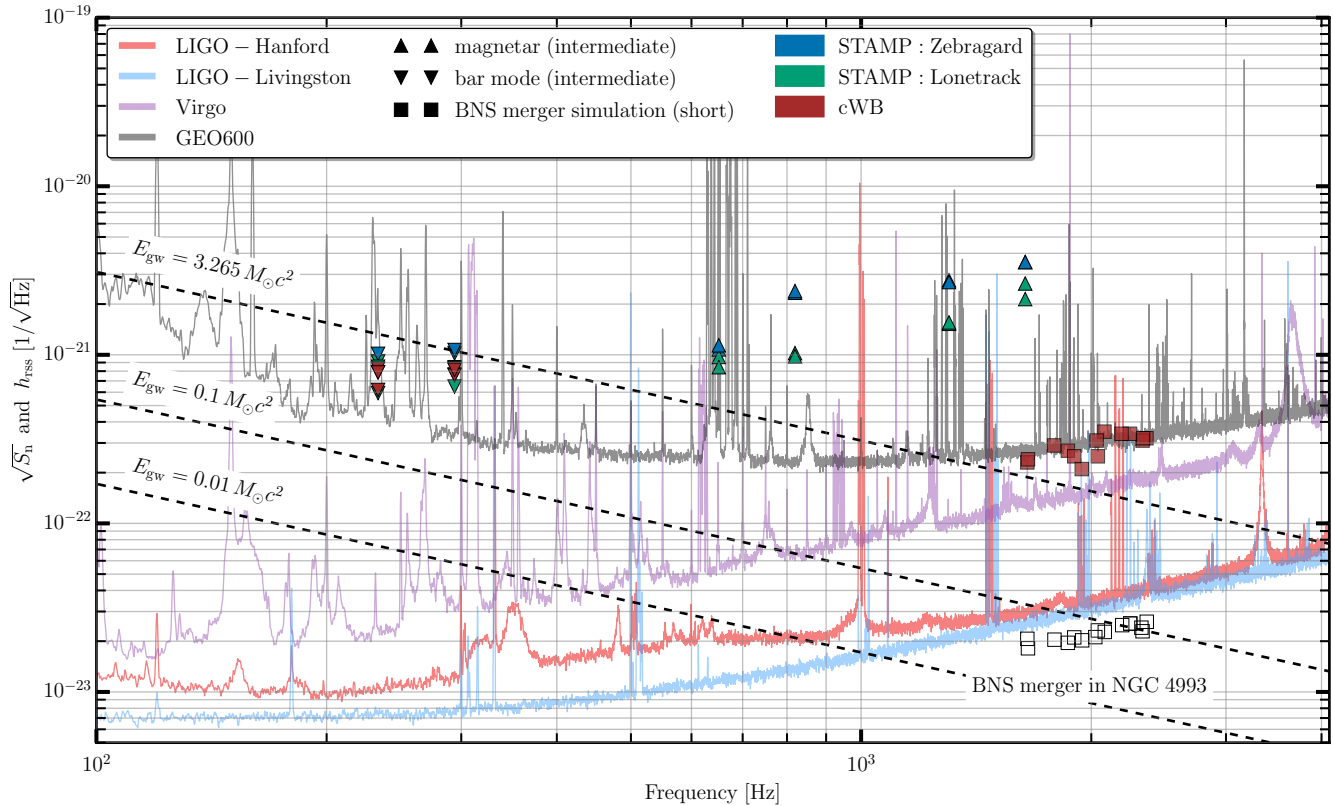


Figure 1. Noise amplitude spectral density $\sqrt{S_n}$ for the four GW detectors (solid curves), and detection efficiency root-sum-square strain amplitudes h_{rss} at 50% false dismissal probability for various waveforms in the short- and intermediate-duration sensitivity studies. The color code of the markers indicates the search, while the marker shapes correspond to the waveform families. The red squares correspond to the short *cWB* analysis, the red triangles to the intermediate-duration *cWB* analysis, and the green and blue triangles correspond to the intermediate-duration *STAMP* Lonetrack and Zebragard analyses respectively. The frequencies on the x-axis correspond to the average frequency of the injected waveform. The short *cWB* analysis fixes the polarization to a value consistent with the pre-merger analysis (Abbott et al. 2017a), while for intermediate durations we marginalize over polarization (see text for details). The top dashed black line indicates the maximum h_{rss} possible for a narrow-band GW signal with fixed energy content E_{gw} , under the most optimistic assumption that the whole energy available after merger is radiated in GWs at a certain frequency. This energy is obtained from the pre-merger analysis (Abbott et al. 2017a) as $E_{\text{gw}} = 3.265 M_{\odot} c^2$ by subtracting the lower bound of $0.025 M_{\odot} c^2$ on the radiated energy from the upper end of the 90% credible range on the total system mass. The region above this line can thus be considered an unphysical part of parameter space, and in reality we expect GW emission of only a fraction of this absolute upper bound – as an example, lines at $0.1 M_{\odot} c^2$ and $0.01 M_{\odot} c^2$ are also shown. The open squares represent the post-merger NR waveforms used in the short *cWB* analysis, but at the h_{rss} assuming the distance and orientation of GW170817 inferred from the pre-merger observation in (Abbott et al. 2017a). Figure produced using matplotlib (Hunter 2007).

310 All NR waveforms have dominant emission well-above
 311 1 kHz, however searching from $f_{\text{min}} = 1024$ Hz is a con-
 312 servative choice made to avoid missing any post-merger
 313 signal content from stiff EOSs but permits pre-merger
 314 and merger-signal content from soft EOSs. In the end,
 315 the search finds no evidence for any GW signal in this
 316 band and the waveforms used to form upper limits are
 317 dominated by the postmerger phase, although they do
 318 allow for some part of the late inspiral and merger.

319 The strains required to produce a 50% probability
 320 of signal detection lie between $2.1 \times 10^{-22} \text{ Hz}^{-1/2}$ and

321 $3.5 \times 10^{-22} \text{ Hz}^{-1/2}$. The GW energy radiated by an
 322 isotropically emitting source is given by Sutton (2013)

$$\begin{aligned}
 E_{\text{gw}}^{\text{iso}} &= \frac{\pi c^3}{2G} \mathcal{D}^2 \int d\Omega \int_{f_{\text{min}}}^{f_{\text{max}}} df f^2 \left(|\tilde{h}_+(f)|^2 + |\tilde{h}_\times(f)|^2 \right) \\
 &\approx \frac{\pi^2 c^3}{G} \mathcal{D}^2 \bar{f}^2 h_{\text{rss}}^2,
 \end{aligned}
 \tag{3}$$

323 where \mathcal{D} is the distance to the source. Using the $h_{\text{rss}}^{50\%}$
 324 sensitivities described above, we find that the energies
 325 to which the search is sensitive are $4.8\text{--}19.6 M_{\odot} c^2$, where
 326 the range corresponds to the variety of waveforms used.

We are therefore not able to constrain post-merger emission from a possible hypermassive NS associated with GW170817.

A separate analysis of the LIGO-Virgo data for unmodelled short duration bursts within a $[-600, +60]$ second window around GRB170817A is reported in Abbott et al. (2017c) using the X-Pipeline package (Sutton et al. 2010; Was et al. 2012). This analysis searched the frequency band 20-1000 Hz. The inspiral phase of GW170817 was detected with a significance of 4.2σ , rising to 5σ when the analysis is constrained to the optical counterpart location. However, no significant events were found following the merger. Limits on the amplitude of GW emission below 1000 Hz are consistent with those reported here.

3.2. Intermediate duration ($\lesssim 500$ s) signals

For intermediate-duration signals, we employ search algorithms adapted from the all-sky searches described in Abbott et al. (2017f). The main difference with respect to the all-sky searches is that instead of searching over many possible sky positions, we again use the known sky position of the optical counterpart. Together with the limited time range to search over, this effectively reduces the number of accidental coincident triggers. Two algorithms are employed: *STAMP* and *cWB*.

While the algorithms are sensitive to rather general waveform morphologies, we test the efficiency of signal recovery for both by a set of specific waveform models to determine $h_{\text{rss}}^{50\%}$. We coherently add these simulated post-merger signals to the data of LIGO Hanford and Livingston covering the on-source period. The waveforms' polarizations are allowed to vary uniformly in ψ and $\cos\iota$, which corresponds to selecting from an isotropic distribution. The sky positions are fixed to the position of the optical transient. We describe the waveform models in the next section.

3.2.1. Waveform Models

Two types of physically-motivated waveform morphologies are considered, corresponding to GWs either from secular bar modes (Lai & Shapiro 1995) or caused by magnetic-field induced ellipticities of the nascent star (Cutler 2002, referred to as *magnetar* waveforms in the following). Another interesting emission mechanism are unstable *r*-modes (Andersson 1998; Mytidis et al. 2015); we do not use such waveforms here due to the duration of their emission, and so searches covering significantly longer timescales will be required.

The secular bar mode is a GW-driven instability (Chandrasekhar 1970; Friedman & Schutz 1975), where the growth timescale of the mode is determined by the ratio of kinetic to binding energy of the star (Lai

& Shapiro 1995). The corresponding waveforms (Corsi & Mészáros 2009) and specific parameters of the model used for the waveforms are given in Appendix A.2 and Table A.2.

The magnetar waveforms assume that the merger results in a star that is rapidly spinning down, whose internal magnetic field has been wound up, generating significant stellar ellipticity (e.g., Cutler 2002; Dall'Osso et al. 2009; Ciolfi & Rezzolla 2013). The star then undergoes a spin-flip instability, causing it to become an orthogonal rotator, and hence maximal emitter of GWs. The specific waveform model is derived in Lasky et al. (2017b). The waveform is parameterized by four parameters: a braking index, stellar ellipticity, the initial GW frequency, and the spindown timescale. Details of these waveforms and their parameters are given in Appendix A.3 and Table A.3.

3.2.2. STAMP

STAMP employs spectrograms with $1\text{ s} \times 1\text{ Hz}$ pixels created from the cross-correlation of data between spatially separated detectors (Thrane et al. 2011), which in this case are LIGO Hanford and LIGO Livingston. We use 500 s spectrograms covering two frequency bands: 24-2000 Hz and 2000-4000 Hz. The on-source data from the time of merger to the end of the second observing run is split into these 500 s spectrograms with 250 s overlap between them. The time-shifted off-source data is taken from August 3, 2017 until the time of the merger. These are searched with both a seed-based clustering method (Zebragard) and with a seedless pattern-recognition algorithm (Lonetrack) that integrates the pixels across tracks which are picked randomly from a large set of Bézier templates over the spectrogram (Thrane & Coughlin 2013; Thrane & Coughlin 2015).

3.2.3. Coherent Wave Burst

For the intermediate-duration search, the *cWB* algorithm (see Sec. 3.1 for algorithm details) searches between 24-2048 Hz using LIGO-Virgo data from the time of the merger to 1000 s later. Selection criteria for candidate gravitational wave triggers are based on the duration of the signal reconstructed by the algorithm as described in Abbott et al. (2017f). The on-source time window is taken to be the time of the merger until 1000 s later, while the off-source data is the period from 13–21 August with the data time-shifted such that no coherent signals remain.

3.2.4. Results

In the *STAMP* analysis, the triggers found in the on-source period are compared to the estimated background of accidental coincident triggers; there is no significant

428 excess of coherent events during this time period in the
 429 24-4000 Hz frequency range searched corresponding to
 430 a 10^{-2} false-alarm probability. Similarly, no GW tran-
 431 sient candidates have been found by *cWB* above a rank-
 432 ing statistic value corresponding to a 10^{-4} false-alarm
 433 probability in the frequency band 24-2048 Hz.

434 We determine detection efficiencies for the models con-
 435 sidered in Sec. 3.2.1. For *STAMP*, we report the equiva-
 436 lent energy released at which the algorithms recover 50%
 437 or more of the injected signals at a false-alarm proba-
 438 bility of 10^{-2} , as well as the corresponding h_{rss} . For
 439 *cWB*, we report the results at a false-alarm probabili-
 440 ty of 10^{-4} . Due to the rapid rise in background events
 441 between false alarm probabilities of 10^{-2} and 10^{-4} , the
 442 results presented here do not depend strongly on this
 443 choice. These false alarm probabilities were chosen as
 444 they correspond to a false alarm rate of approximately
 445 1 per year. The best *STAMP* results correspond to
 446 an $h_{\text{rss}}^{50\%} = 5.9 \times 10^{-22} \text{ Hz}^{-1/2}$ with equivalent energy
 447 of $E_{\text{GW}} = 2 M_{\odot} c^2$ for the bar-mode signal models.
 448 The results for the *cWB* analysis are similar. For the
 449 magnetar signal models, the best *STAMP* results are
 450 $h_{\text{rss}}^{50\%} = 8.4 \times 10^{-22} \text{ Hz}^{-1/2}$ and $E_{\text{GW}} = 4 M_{\odot} c^2$. *cWB*
 451 did not analyze these waveforms. The energy limits are
 452 computed using Eq. 3 where isotropic GW emission is
 453 assumed and the $h_{\text{rss}}^{50\%}$ values are marginalized over po-
 454 larization.

455 4. IMPLICATIONS AND CONCLUSIONS

456 We report on a search for GWs from the post-
 457 merger remnant following the binary NS coalescence
 458 GW170817, using robust and generic time-frequency
 459 excess power analysis methods. Such GWs can come
 460 from a short-lived hypermassive NS lasting $\lesssim 1$ s before
 461 collapsing to a BH or from a longer-lived supramassive
 462 or stable NS. We find no evidence in our data for GWs
 463 after the merger of GW170817. If a signal exists, it is
 464 too weak to be detected with current sensitivity and
 465 analysis algorithms.

466 For the data set and methods employed in this paper,
 467 we find search sensitivities, in terms of GW signal am-
 468 plitude, that are approximately an order of magnitude
 469 from expectations for GW emission in the literature. For
 470 example, short-lived hypermassive NSs are expected to
 471 emit a few percent of a solar mass in gravitational-wave
 472 energy (e.g., see the two lower dashed lines in Fig. 1
 473 that represent 1% and 10% of a solar mass; Kiuchi et al.
 474 2009; Clark et al. 2014; Bernuzzi et al. 2015b; Endrizzi
 475 et al. 2016; Dietrich et al. 2017a,b; Feo et al. 2017),
 476 while our minimum 50% efficiency is $E_{\text{GW}} \lesssim 4.8 M_{\odot} c^2$
 477 (see Sec. 3.1). Gravitational-wave emission from a rep-
 478 resentative sample of these numerical relativity simu-

479 lations are shown as open squares in Fig. 1, which
 480 are approximately an order of magnitude in strain be-
 481 low the $h_{\text{rss}}^{50\%}$ points for the corresponding waveforms
 482 (filled squares). For intermediate-duration signals from
 483 supramassive or stable NSs (Sec. 3.2), we find a min-
 484 imum of $E_{\text{GW}} \lesssim 4 M_{\odot} c^2$ for the millisecond magnetar
 485 model (Lasky et al. 2017b), and $E_{\text{GW}} \lesssim 2 M_{\odot} c^2$ for the
 486 model describing secular bar modes (Corsi & Mészáros
 487 2009).

488 Figure 1 shows the $h_{\text{rss}}^{50\%}$ for the considered waveform
 489 models as a function of the waveform’s signal-weighted
 490 frequency. Based on this, the distance of 40 Mpc for
 491 the binary NS is approximately an order of magnitude
 492 greater than the distances to which we are sensitive.
 493 This gives significant motivation to continue searching
 494 for intermediate-duration post-merger remnants in later
 495 iterations of the advanced (or future) GW detectors as
 496 well as the development of improved analysis methods.

497 GW170817 was detected in the second observing run
 498 of the advanced GW detectors. Further improvements
 499 towards their design sensitivity are now underway (Ab-
 500 bott et al. 2016a). At design sensitivity, a matched-
 501 filter search with precisely modelled post-merger wave-
 502 forms could detect signals from a hypermassive NS rem-
 503 nant out to distances of ~ 20 –40 Mpc (computed as
 504 the single-detector horizon distance for a signal-to-noise
 505 threshold of 5) (Takami et al. 2014; Clark et al. 2016).
 506 Conversely, with current detector sensitivities and the
 507 more robust search methods not relying on matched fil-
 508 tering that are employed in this paper, a post-merger
 509 detection for GW170817 is not very likely a priori, but
 510 the theoretical uncertainties still make a search impor-
 511 tant. By using algorithms designed to be sensitive to
 512 generic signals, the searches are robust to these theoret-
 513 ical uncertainties and capable of detection of unmodeled
 514 signals.

515 This study motivates increased research and develop-
 516 ment towards improved sensitivity at high-frequencies in
 517 current instruments, planned upgrades and also third-
 518 generation interferometers. Future improvements can
 519 also be made to the search methods presented in this
 520 paper. For example, in searching for short-duration
 521 signals, the sparsity of numerical-relativity waveforms
 522 makes it challenging to perform matched-filter searches
 523 for the inspiral, merger and hypermassive phases. How-
 524 ever, the dominant post-merger GW modes are dictated
 525 by only a few pre-merger parameters and the equation
 526 of state (e.g., Read et al. 2013; Bernuzzi et al. 2015a;
 527 Bauswein & Stergioulas 2015; Rezzolla & Takami 2016),
 528 implying more sensitive techniques can be developed
 529 that use parameters measured during the inspiral to

inform priors on the physical parameters of the post-merger remnant.

A full matched-filter search is likely not computationally possible for intermediate-duration signals due to the large parameter spaces and theoretical uncertainties involved with the waveforms. However, sensitivity can be improved by targetting specific emission models (e.g., [Coyne et al. 2016](#)).

A search for longer-duration ($\gtrsim 1$ day) remnant signals is also planned, with the maximum detectable signal length limited by the 7.9 days of data available following the merger until the official end of the LIGO-Virgo second observing run. A variant of the intermediate-duration algorithms with different pixel sizes can be used to create spectrograms that cover the full duration of the analysis, making it more sensitive to longer-lived signals than the maps employed here ([Thrane et al. 2015](#)). Moreover, a variety of methods have been developed to search for persistent, nearly-monochromatic signals from mature NSs (see [Prix 2009](#); [Riles 2013](#); [Bejger 2017](#), for reviews). Several of these could be modified to search for a long-lived post-merger signal, though the expected rapid decrease in frequency is likely to pose technical challenges to current algorithms.

In addition to improving the sensitivity to potential post-merger signals of GW170817, another important program is to improve our ability to detect post-merger GWs from future LIGO/Virgo discoveries of binary NS mergers. At design sensitivity, Advanced LIGO and Advanced Virgo both aim to be approximately a factor three better in broadband sensitivity than during the second observing run ([Abbott et al. 2016a](#)), and next generation detectors will improve the sensitivities significantly beyond that. This provides a number of opportunities. Clearly, increased sensitivity in the \gtrsim kHz range implies improved ability to detect single post-merger signals. Moreover, increased broadband sensitivity implies higher rates of binary NS inspiral and merger detections, and hence might make possible power or coherent stacking of events to increase our sensitivity to post-merger physics ([Bose et al. 2017](#); [Yang et al. 2017](#)).

The authors gratefully acknowledge the support of the United States National Science Foundation (NSF) for the construction and operation of the LIGO Laboratory and Advanced LIGO as well as the Science and Technology Facilities Council (STFC) of the United Kingdom, the Max-Planck-Society (MPS), and the State of

Niedersachsen/Germany for support of the construction of Advanced LIGO and construction and operation of the GEO600 detector. Additional support for Advanced LIGO was provided by the Australian Research Council. The authors gratefully acknowledge the Italian Istituto Nazionale di Fisica Nucleare (INFN), the French Centre National de la Recherche Scientifique (CNRS) and the Foundation for Fundamental Research on Matter supported by the Netherlands Organisation for Scientific Research, for the construction and operation of the Virgo detector and the creation and support of the EGO consortium. The authors also gratefully acknowledge research support from these agencies as well as by the Council of Scientific and Industrial Research of India, the Department of Science and Technology, India, the Science & Engineering Research Board (SERB), India, the Ministry of Human Resource Development, India, the Spanish Agencia Estatal de Investigación, the Vicepresidència i Conselleria d’Innovació, Recerca i Turisme and the Conselleria d’Educació i Universitat del Govern de les Illes Balears, the Conselleria d’Educació, Investigació, Cultura i Esport de la Generalitat Valenciana, the National Science Centre of Poland, the Swiss National Science Foundation (SNSF), the Russian Foundation for Basic Research, the Russian Science Foundation, the European Commission, the European Regional Development Funds (ERDF), the Royal Society, the Scottish Funding Council, the Scottish Universities Physics Alliance, the Hungarian Scientific Research Fund (OTKA), the Lyon Institute of Origins (LIO), the National Research, Development and Innovation Office Hungary (NKFI), the National Research Foundation of Korea, Industry Canada and the Province of Ontario through the Ministry of Economic Development and Innovation, the Natural Science and Engineering Research Council Canada, the Canadian Institute for Advanced Research, the Brazilian Ministry of Science, Technology, Innovations, and Communications, the International Center for Theoretical Physics South American Institute for Fundamental Research (ICTP-SAIFR), the Research Grants Council of Hong Kong, the National Natural Science Foundation of China (NSFC), the Leverhulme Trust, the Research Corporation, the Ministry of Science and Technology (MOST), Taiwan and the Kavli Foundation. The authors gratefully acknowledge the support of the NSF, STFC, MPS, INFN, CNRS and the State of Niedersachsen/Germany for provision of computational resources.

APPENDIX

A. WAVEFORMS

Here we provide details of the waveform models used to determine the detection efficiency of our search algorithms. For short-duration signals (Sec. 3.1) we use simulations of binary NS mergers. For intermediate durations (Sec. 3.2.1), we use two models: secular bar modes and magnetar waveforms.

A.1. Binary neutron star waveforms

We determine the efficacy of the short-duration *cWB* analysis (Sec. 3.1) through Monte-Carlo simulations using GW waveforms derived from simulations of binary NS systems that include a post-merger phase. Table A.1 provides a summary of the waveforms in terms of their expected h_{rSS} for a binary NS at 40 Mpc and the h_{rSS} required for 50% detection efficiency by *cWB* with a 10^{-4} false-alarm probability, $h_{\text{rSS}}^{50\%}$.

Equation of state	m_1	m_2	\bar{f}	Simulation	h_{rSS} (expected)	$h_{\text{rSS}}^{50\%}$
	[M_\odot]	[M_\odot]	[Hz]		[$10^{-22}/\sqrt{\text{Hz}}$]	[$10^{-22}/\sqrt{\text{Hz}}$]
H4 (Glendenning & Moszkowski 1991)	1.25	1.25	1946	Takami et al. (2015)	0.21	2.1
H4 (Glendenning & Moszkowski 1991)	1.3	1.3	2083	Takami et al. (2015)	0.23	3.5
H4 (Glendenning & Moszkowski 1991)	1.35	1.35	2247	Ciolfi et al. (2017)	0.26	3.4
H4 (Glendenning & Moszkowski 1991)	1.42	1.29	2192	Ciolfi et al. (2017)	0.26	3.4
H4 (Glendenning & Moszkowski 1991)	1.54	1.26	2030	Kawamura et al. (2016)	0.22	3.1
LS220 (Lattimer & Swesty 1991)	1.20	1.50	1900	Bauswein et al. (2013a)	0.22	2.5
SHT (Shen et al. 2010)	1.40	1.40	1788	Kastaun et al. (2017)	0.21	2.9
SFHx (Steiner et al. 2013)	1.2	1.5	1650	Bauswein et al. (2013a)	0.21	2.3
SFHx (Steiner et al. 2013)	1.35	1.35	2040	Bauswein et al. (2013a)	0.24	2.5
SLy (Douchin & Haensel 2001)	1.25	1.25	2333	Takami et al. (2015)	0.23	3.2
SLy (Douchin & Haensel 2001)	1.3	1.3	2325	Takami et al. (2015)	0.25	3.1
SLy (Douchin & Haensel 2001)	1.35	1.25	2363	Takami et al. (2015)	0.27	3.2
TMA (Toki et al. 1995)	1.20	1.50	1864	Bauswein et al. (2013a)	0.19	3.2
TMA (Toki et al. 1995)	1.35	1.35	1653	Bauswein et al. (2013a)	0.20	2.4

Table 1. Sensitivity of the *cWB* pipeline to waveforms generated by binary NS simulations. Waveforms were selected to represent a variety of equations of state (first column) and progenitor mass configurations (second and third columns). The fourth column is the mean frequency for each waveform \bar{f} , and the fifth column is the reference for the BNS simulation. The sixth column is the root-sum-squared strain h_{rSS} predicted by that simulation for a post-merger signal from a BNS with distance and inclination consistent with estimates from the inspiral analysis (Abbott et al. 2017a). The seventh column shows the h_{rSS} required for 50% detection efficiency with a false-alarm probability of 10^{-4} , $h_{\text{rSS}}^{50\%}$.

A.2. Secular bar mode waveforms

Long-lived post-merger remnants may be unstable due to the secular bar-mode instability. This instability occurs when the ratio of rotational kinetic energy to gravitational binding energy $T/|W|$ is in the range $0.14 < T/|W| < 0.27$ (Lai & Shapiro 1995). For all injected waveforms used in this study we follow the treatment described in Corsi & Mészáros (2009), which we briefly summarize. We set $T/|W| = 0.2$ for the kinetic-to-gravitational potential energy ratio of the initial axisymmetric configuration (in the middle of the secular instability range). The NS spin-down is then determined by the combination of magnetic dipole and GW losses (Corsi & Mészáros 2009):

$$\frac{dE}{dt} = -\frac{B^2 R^6 \Omega_{\text{eff}}^4}{6c^3} - \frac{32GI^2 \epsilon^2 \Omega^6}{5c^5}. \quad (\text{A1})$$

Here, B is the star’s dipolar field strength at the poles, R is the mean stellar radius (i.e. the geometric mean of the principal axes of the star), Ω is the star’s angular frequency, Ω_{eff} is the effective angular frequency (which includes the effect of internal fluid motions), ϵ is the ellipticity, and I is the moment of inertia with respect to the rotation axis. The GW strain is then

$$h(t) = \frac{4G}{c^4} \frac{I\epsilon\Omega^2}{\mathcal{D}}, \quad (\text{A2})$$

where Ω is found by integrating Eqn. (A1).

For all injected waveforms we assume a total NS mass of $2.6 M_{\odot}$, which is close to the lower bound of the estimated total mass range for GW170817 ($2.73 M_{\odot}$; see Abbott et al. 2017a) and to the lower bound of $2.57 M_{\odot}$ for the total mass of other known binary NS systems (see Abbott et al. 2017a, and references therein). For a given initial $T/|W|$ value, the total radiated energy during the secular bar-mode evolution scales as M^2 (see e.g. Fig. 3 in Lai & Shapiro 1995), implying that our value of the mass can be regarded as conservative within the (optimistic) assumption that all of the total mass of the binary goes into the post-merger remnant. We use a range of magnetic field values from 10^{13} to 5×10^{14} G. Fields higher than $\sim 10^{15}$ G result in rapid spindown of the star, and hence uninteresting GW amplitudes; fields lower than $\sim 10^{13}$ G are unrealistic for such systems given the post-merger remnant dynamics that wind up strong fields. Because we do not know the ultimate fate of the bar-shaped remnant, and whether it can survive up to the ultimate Dedekind configuration (Lai & Shapiro 1995), we only evolve waveforms up to a time when the luminosity emitted in GWs is 1% of the peak value, which is sufficient to capture the bulk of the energy emitted in GWs. Table A.2 shows the specific parameters used for our waveforms, as well as h_{rss} at 50% efficiency computed at a fixed false alarm probability for each of the pipelines used in this search. These results are also shown in Fig. 1.

Properties					$h_{\text{rss}}^{50\%} [10^{-22}/\sqrt{\text{Hz}}]$		
R	B	T	f_0	f_f	cWB	$STAMP$	
[km]	[G]	[s]	[Hz]	[Hz]		Lonetrack	Zebragard
12	10^{13}	277	449	139	8.3	8.4	10
12	10^{14}	237	449	139	8.3	9.0	9.2
12	5×10^{14}	107	449	139	7.6	6.5	7.6
14	10^{13}	509	356	111	7.9	8.1	10
14	10^{14}	396	356	111	8.1	8.3	11
14	5×10^{14}	136	356	111	6.2	5.9	7.9

Table 2. h_{rss} at 50% efficiency to the bar mode waveforms computed for a false-alarm probability of 10^{-2} for $STAMP$ and 10^{-4} for cWB —see Sec. 3.2. Here, B is the star’s dipolar magnetic field strength at the pole, R the mean stellar radius, T the duration of the waveform in seconds, and f_0 and f_f define the beginning and end of the frequency range where the bulk of the GW energy is emitted. Please see Sec. A.2 for further waveform details.

A.3. Magnetar waveforms

Gravitational waveforms from spinning-down nascent NSs with arbitrary braking index are derived in Lasky et al. (2017b). Here we assume that the rotational evolution of the star is described by the torque equation: $\dot{\Omega} \propto \Omega^n$, where n is the braking index. Integrating the torque equation enables one to derive the star’s spin evolution, and hence the GW frequency

$$f(t) = f_0 \left(1 + \frac{t}{\tau} \right)^{1/(1-n)}, \quad (\text{A3})$$

where f_0 is the initial GW frequency, and τ is the spindown timescale. The gravitational-wave strain is then given by Eqn. (A2), where the GW frequency is twice the star’s spin frequency.

A braking index of $n = 5$ represents gravitational-wave driven spindown due to stellar ellipticity ϵ , whereas an unchanging dipolar magnetic field in vacuum induces a braking index of $n = 3$. Observations of X-ray afterglows

655 from short GRBs allow for constraints on τ and $\Omega(t=0)$, and hence f_0 (Rowlinson et al. 2013), as well as ϵ (Lasky
656 & Glampedakis 2016), and n (Lasky et al. 2017a). The braking index of two millisecond magnetars have been
657 measured, both below 3; we therefore choose $n = 2.5$ and $n = 5$ to adequately sample the space. Empirically,
658 such stellar ellipticities are limited to $\lesssim 10^{-2}$, although theoretically such a large value is difficult to generate with
659 internal magnetic fields as it requires a field of $\sim 10^{17}$ G. Large-scale α - Ω dynamos may generate internal fields
660 of $\sim 10^{16}$ G (Thompson & Duncan 1993), with small-scale turbulent dynamos potentially amplifying the field to
661 $\lesssim 5 \times 10^{16}$ G (Zrake & MacFadyen 2013), implying ellipticities as high as $\approx 2.5 \times 10^{-3}$ (Cutler 2002). In principle, the
662 ellipticity should effect the GW frequency evolution, however in these waveform models that factor is absorbed into
663 τ . Finally, while X-ray observations indicate $10 \lesssim \tau/s \lesssim 10^5$ (Rowlinson et al. 2013), we only show waveform results
664 here using $\tau = 100$ s as larger τ yields uninteresting GW limits.

665 Table A.3 shows waveform parameters used in this study and corresponding h_{rss} at 50% efficiency computed for
666 a fixed false alarm probability of 10^{-2} . We do not list the duration of the waveform as all magnetar waveforms are
667 longer than the search duration.

Properties				$h_{\text{rss}}^{50\%} [10^{-22}/\sqrt{\text{Hz}}]$	
ϵ	n	f_0	f_{500}	STAMP	
		[Hz]	[Hz]	Lonetrack	ZebraGard
0.01	2.5	1000	303	9.7	11
0.001	2.5	1000	303	8.4	11
0.01	5	1000	639	10	23
0.001	5	1000	639	9.8	24
0.01	2.5	2000	606	15	28
0.001	2.5	2000	606	16	27
0.01	5	2000	1278	26	35
0.001	5	2000	1278	21	35

Table 3. h_{rss} at 50% efficiency to the magnetar waveforms computed for a false-alarm probability of 10^{-2} for the STAMP pipelines used in the intermediate-duration search—see Sec. 3.2. The first four columns are respectively the stellar ellipticity ϵ , the braking index n , the initial GW frequency f_0 , and the GW frequency after 500 s f_{500} , which is the duration of the analyses. Please see Sec. A.3 for further waveform details.

REFERENCES

- 668 Aasi, J., et al. 2015, *Classical and Quantum Gravity*, 32,
669 074001
- 670 Abbott, B. P., et al. 2016a, *Living Reviews in Relativity*,
671 19, 1
- 672 —. 2016b, *Classical & Quantum Gravity*, 33, 134001
- 673 Abbott, B. P., et al. 2017a, *Physical Review Letters*, 119,
674 161101
- 675 —. 2017b, *Astrophysical Journal Letters*, 848, L12
- 676 —. 2017c, *Astrophysical Journal Letters*, 848, L13
- 677 —. 2017d, *Nature*, advance online publication, .
678 <http://dx.doi.org/10.1038/nature24471>
- 679 —. 2017e, *Astrophysical Journal Letters* (accepted),
680 arXiv:1710.05836
- 681 —. 2017f, all-sky search for long duration
682 gravitational-wave transients in the first Advanced LIGO
683 run, in preparation
- 684 Acernese, F., et al. 2015, *Classical and Quantum Gravity*,
685 32, 024001
- 686 Anderson, W. G., Brady, P. R., Creighton, J. D. E., &
687 Flanagan, E. E. 2000, *Int. J. Mod. Phys.*, D9, 303
- 688 Andersson, N. 1998, *ApJ*, 502, 708
- 689 Baiotti, L., Giacomazzo, B., & Rezzolla, L. 2008, *Phys.*
690 *Rev.*, D78, 084033
- 691 Baiotti, L., Hawke, I., & Rezzolla, L. 2007, *Classical and*
692 *Quantum Gravity*, 24, S187
- 693 Baumgarte, T. W., Shapiro, S. L., & Shibata, M. 2000,
694 *Astrophysical Journal Letters*, 528, L29

- 695 Bauswein, A., Baumgarte, T. W., & Janka, H.-T. 2013a,
696 Physical Review Letters, 111, 131101
- 697 Bauswein, A., Goriely, S., & Janka, H.-T. 2013b,
698 Astrophysical Journal , 773, 78
- 699 Bauswein, A., & Janka, H. T. 2012, Phys. Rev. Lett., 108,
700 011101
- 701 Bauswein, A., & Stergioulas, N. 2015, Physical Review D ,
702 91, 124056
- 703 Bejger, M. 2017, in Proceedings of the 52nd Rencontres de
704 Moriond: Gravitation
- 705 Berger, E. 2014, Annual Reviews of Astronomy &
706 Astrophysics, 52, 43
- 707 Bernuzzi, S., Dietrich, T., & Nagar, A. 2015a, Physical
708 Review Letters, 115, 091101
- 709 Bernuzzi, S., Nagar, A., Balmelli, S., Dietrich, T., & Ujevic,
710 M. 2014, Phys. Rev. Lett., 112, 201101
- 711 Bernuzzi, S., Nagar, A., Dietrich, T., & Damour, T. 2015b,
712 Physical Review Letters, 114, 161103
- 713 Bonazzola, S., & Gourgoulhon, E. 1996, Astron.
714 Astrophys., 312, 675
- 715 Bose, S., Chakravarti, K., Rezzolla, L., Sathyaprakash,
716 B. S., & Takami, K. 2017, ArXiv e-prints,
717 arXiv:1705.10850
- 718 Cahillane, C., et al. 2017, arXiv:1708.03023
- 719 Chandrasekhar, S. 1970, Phys. Rev. Lett., 24, 611
- 720 Ciolfi, R., Kastaun, W., Giacomazzo, B., et al. 2017,
721 Physical Review D , 95, 063016
- 722 Ciolfi, R., & Rezzolla, L. 2013, MNRAS , 435, L43
- 723 Clark, J., Bauswein, A., Cadonati, L., et al. 2014, Physical
724 Review D , 90, 062004
- 725 Clark, J. A., Bauswein, A., Stergioulas, N., & Shoemaker,
726 D. 2016, Classical and Quantum Gravity, 33, 085003
- 727 Cornish, N. J., & Littenberg, T. B. 2015, Classical and
728 Quantum Gravity, 32, 135012
- 729 Corsi, A., & Mészáros, P. 2009, Astrophysical Journal , 702,
730 1171
- 731 Coulter et al. 2017, Science, doi:10.1126/science.aap9811
- 732 Coyne, R., Corsi, A., & Owen, B. J. 2016, Phys. Rev. D,
733 93, 104059
- 734 Cutler, C. 2002, Phys. Rev. D, 66, 084025
- 735 Dall’Osso, S., Giacomazzo, B., Perna, R., & Stella, L. 2015,
736 The Astrophysical Journal, 798, 25
- 737 Dall’Osso, S., Shore, S. N., & Stella, L. 2009, Monthly
738 Notices of the Royal Astronomical Society, 398, 1869
- 739 Dietrich, T., Bernuzzi, S., Ujevic, M., & Tichy, W. 2017a,
740 Phys. Rev. D, 95, 044045
- 741 Dietrich, T., Ujevic, M., Tichy, W., Bernuzzi, S., &
742 Brüggmann, B. 2017b, Phys. Rev. D, 95, 024029
- 743 Doneva, D. D., Kokkotas, K. D., & Pnigouras, P. 2015,
744 Phys. Rev. D, 92, 104040
- 745 Dooley, K. L., Leong, J. R., Adams, T., et al. 2016,
746 Classical and Quantum Gravity, 33, 075009
- 747 Douchin, F., & Haensel, P. 2001, Astronomy &
748 Astrophysics, 380, 151
- 749 Driggers, J. C., et al. 2017, Offline noise subtraction for
750 Advanced LIGO, Tech. Rep. LIGO-P1700260.
751 <https://dcc.ligo.org/P1700260/public>
- 752 Endrizzi, A., Ciolfi, R., Giacomazzo, B., Kastaun, W., &
753 Kawamura, T. 2016, Classical and Quantum Gravity, 33,
754 164001
- 755 Evans, P., et al. 2017, Science, 359,
756 doi:10.1126/science.aap9580
- 757 Fan, Y.-Z., Wu, X.-F., & Wei, D.-M. 2013, Phys. Rev. D,
758 88, 067304
- 759 Feo, A., De Pietri, R., Maione, F., & Löffler, F. 2017,
760 Classical and Quantum Gravity, 34, 034001
- 761 Friedman, J. L., & Schutz, B. F. 1975, Astrophys. J., 199,
762 L157
- 763 Glendenning, N. K., & Moszkowski, S. A. 1991, Phys. Rev.
764 Lett., 67, 2414
- 765 Goldstein, A., et al. 2017, Astrophysical Journal Letters,
766 848, L14
- 767 Hotokezaka, K., Kiuchi, K., Kyutoku, K., et al. 2013,
768 Physical Review D , 88, 044026
- 769 Hunter, J. D. 2007, Computing In Science & Engineering,
770 9, 90
- 771 Kastaun, W., Ciolfi, R., Endrizzi, A., & Giacomazzo, B.
772 2017, Phys. Rev. D, 96, 043019
- 773 Kastaun, W., & Galeazzi, F. 2015, Physical Review D , 91,
774 064027
- 775 Kawamura, T., Giacomazzo, B., Kastaun, W., et al. 2016,
776 Physical Review D , 94, 064012
- 777 Kiuchi, K., Sekiguchi, Y., Shibata, M., & Taniguchi, K.
778 2009, Phys. Rev. D, 80, 064037
- 779 Klimenko, S., & Mitselmakher, G. 2004, Class. Quant.
780 Grav., 21, S1819
- 781 Klimenko, S., Vedovato, G., Drago, M., et al. 2016, Phys.
782 Rev. D, 93, 042004
- 783 Lai, D., & Shapiro, S. L. 1995, ApJ, 442, 259
- 784 Lasky, P. D., & Glampedakis, K. 2016, MNRAS , 458, 1660
- 785 Lasky, P. D., Leris, C., Rowlinson, A., & Glampedakis, K.
786 2017a, Astrophysical Journal Letters, 843, L1
- 787 Lasky, P. D., Sarin, N., & Sammut, L. 2017b,
788 Long-duration waveform models for millisecond
789 magnetars born in binary neutron star mergers, Tech.
790 rep., <https://dcc.ligo.org/LIGO-T1700408>
- 791 Lattimer, J. M., & Swesty, F. D. 1991, Nucl. Phys. A, 535,
792 331
- 793 Lindblom, L., Owen, B. J., & Morsink, S. M. 1998, Physical
794 Review Letters, 80, 4843

- 795 Lü, H.-J., Zhang, B., Lei, W.-H., Li, Y., & Lasky, P. D.
796 2015, *Astrophysical Journal* , 805, 89
- 797 Maione, F., De Pietri, R., Feo, A., & Löffler, F. 2017,
798 *Physical Review D* , 96, 063011
- 799 Metzger, B. D., & Fernández, R. 2014, *MNRAS* , 441, 3444
- 800 Mytidis, A., Coughlin, M., & Whiting, B. 2015, *The*
801 *Astrophysical Journal*, 810, 27
- 802 Palomba, C. 2001, *Astronomy and Astrophysics*, 367, 525
- 803 Prix, R. 2009, *ASSL*, Vol. 357, *Gravitational Waves from*
804 *Spinning Neutron Stars*, ed. W. Becker (Springer Berlin
805 Heidelberg), 651–685.
806 <https://dcc.ligo.org/LIGO-P060039/public>
- 807 Ravi, V., & Lasky, P. D. 2014, *MNRAS* , 441, 2433
- 808 Read, J. S., Baiotti, L., Creighton, J. D. E., et al. 2013,
809 *Physical Review D* , 88, 044042
- 810 Rezzolla, L., & Takami, K. 2016, *Physical Review D* , 93,
811 124051
- 812 Riles, K. 2013, *Prog. Part. Nucl. Phys.*, 68, 1
- 813 Rowlinson, A., O’Brien, P. T., Metzger, B. D., Tanvir,
814 N. R., & Levan, A. J. 2013, *MNRAS* , 430, 1061
- 815 Ruffert, M., Janka, H.-T., & Schaefer, G. 1996, *Astronomy*
816 *& Astrophysics*, 311, 532
- 817 Shapiro, S. L. 2000, *Astrophysical Journal* , 544, 397
- 818 Shen, G., Horowitz, C. J., & Teige, S. 2010, *Phys. Rev. C*,
819 82, 015806
- 820 Shibata, M. 2005, *Physical Review Letters*, 94, 201101
- 821 Shibata, M., & Taniguchi, K. 2006, *Physical Review D* , 73,
822 064027
- 823 Shibata, M., & Uryū, K. b. o. 2000, *Phys. Rev. D*, 61,
824 064001
- 825 Smartt, S. J., et al. 2017, *Nature*, doi:10.1038/nature24303
- 826 Steiner, A. W., Hempel, M., & Fischer, T. 2013, *Astrophys.*
827 *J.*, 774, 17
- 828 Sutton, P. J. 2013, *ArXiv e-prints*, arXiv:1304.0210
- 829 Sutton, P. J., Jones, G., Chatterji, S., et al. 2010, *New*
830 *Journal of Physics*, 12, 053034
- 831 Takami, K., Rezzolla, L., & Baiotti, L. 2014, *Physical*
832 *Review Letters*, 113, 091104
- 833 —. 2015, *Physical Review D* , 91, 064001
- 834 Thompson, C., & Duncan, R. C. 1993, *Astrophysical*
835 *Journal* , 408, 194
- 836 Thrane, E., & Coughlin, M. 2013, *Physical Review D* , 88,
837 083010
- 838 Thrane, E., & Coughlin, M. 2015, *Phys. Rev. Lett.*, 115,
839 181102
- 840 Thrane, E., Mandic, V., & Christensen, N. 2015, *Physical*
841 *Review D*, 91, doi:10.1103/PhysRevD.91.104021, arXiv:
842 1501.06648
- 843 Thrane, E., Kandhasamy, S., Ott, C. D., et al. 2011,
844 *Physical Review D*, 83, doi:10.1103/PhysRevD.83.083004,
845 arXiv: 1012.2150
- 846 Toki, H., Hirata, D., Sugahara, Y., Sumiyoshi, K., &
847 Tanihata, I. 1995, *Nuclear Physics A*, 588, 357
- 848 Troja, E., Piro, L., van Eerten, H., et al. 2017, *Nature*,
849 advance online publication, .
850 <http://dx.doi.org/10.1038/nature24290>
- 851 Was, M., Sutton, P. J., Jones, G., & Leonor, I. 2012, *Phys.*
852 *Rev. D*, 86, 022003. [https:](https://link.aps.org/doi/10.1103/PhysRevD.86.022003)
853 [//link.aps.org/doi/10.1103/PhysRevD.86.022003](https://link.aps.org/doi/10.1103/PhysRevD.86.022003)
- 854 Xing, Z.-G., Centrella, J. M., & McMillan, S. L. W. 1994,
855 *Phys. Rev.*, D50, 6247
- 856 Yang, H., Paschalidis, V., Yagi, K., et al. 2017, *ArXiv*
857 *e-prints*, arXiv:1707.00207
- 858 Zrake, J., & MacFadyen, A. I. 2013, *Astrophysical Journal*
859 *Letters*, 769, L29

860 THE LIGO SCIENTIFIC COLLABORATION, THE VIRGO COLLABORATION, B. P. ABBOTT,¹ R. ABBOTT,¹ T. D. ABBOTT,²
 861 F. ACERNESE,^{3,4} K. ACKLEY,^{5,6} C. ADAMS,⁷ T. ADAMS,⁸ P. ADESSO,⁹ R. X. ADHIKARI,¹ V. B. ADYA,¹⁰ C. AFFELDT,¹⁰
 862 M. AFROUGH,¹¹ B. AGARWAL,¹² M. AGATHOS,¹³ K. AGATSUMA,¹⁴ N. AGGARWAL,¹⁵ O. D. AGUIAR,¹⁶ L. AIELLO,^{17,18}
 863 A. AIN,¹⁹ P. AJITH,²⁰ B. ALLEN,^{10,21,22} G. ALLEN,¹² A. ALLOCCA,^{23,24} P. A. ALTIN,²⁵ A. AMATO,²⁶ A. ANANYEVA,¹
 864 S. B. ANDERSON,¹ W. G. ANDERSON,²¹ S. V. ANGELOVA,²⁷ S. ANTIER,²⁸ S. APPERT,¹ K. ARAI,¹ M. C. ARAYA,¹
 865 J. S. AREEDA,²⁹ N. ARNAUD,^{28,30} K. G. ARUN,³¹ S. ASCENZI,^{32,33} G. ASHTON,¹⁰ M. AST,³⁴ S. M. ASTON,⁷ P. ASTONE,³⁵
 866 D. V. ATALLAH,³⁶ P. AUFMUTH,²² C. AULBERT,¹⁰ K. AULTONEAL,³⁷ C. AUSTIN,² A. AVILA-ALVAREZ,²⁹ S. BABAK,³⁸
 867 P. BACON,³⁹ M. K. M. BADER,¹⁴ S. BAE,⁴⁰ P. T. BAKER,⁴¹ F. BALDACCINI,^{42,43} G. BALLARDIN,³⁰ S. BANAGIRI,⁴⁴
 868 J. C. BARAYOGA,¹ S. E. BARCLAY,⁴⁵ B. C. BARISH,¹ D. BARKER,⁴⁶ K. BARKETT,⁴⁷ F. BARONE,^{3,4} B. BARR,⁴⁵
 869 L. BARSOTTI,¹⁵ M. BARSUGLIA,³⁹ D. BARTA,⁴⁸ J. BARTLETT,⁴⁶ I. BARTOS,^{49,5} R. BASSIRI,⁵⁰ A. BASTI,^{23,24} J. C. BATCH,⁴⁶
 870 M. BAWAJ,^{51,43} J. C. BAYLEY,⁴⁵ M. BAZZAN,^{52,53} B. BÉCSY,⁵⁴ C. BEER,¹⁰ M. BEJGER,⁵⁵ I. BELAHCENE,²⁸ A. S. BELL,⁴⁵
 871 G. BERGMANN,¹⁰ S. BERNUZZI,^{56,57} J. J. BERO,⁵⁸ C. P. L. BERRY,⁵⁹ D. BERSANETTI,⁶⁰ A. BERTOLINI,¹⁴ J. BETZWIESER,⁷
 872 S. BHAGWAT,⁶¹ R. BHANDARE,⁶² I. A. BILENKO,⁶³ G. BILLINGSLEY,¹ C. R. BILLMAN,⁵ J. BIRCH,⁷ R. BIRNEY,⁶⁴
 873 O. BIRNHOLTZ,¹⁰ S. BISCANS,^{1,15} S. BISCOVEANU,^{65,6} A. BISHT,²² M. BITOSI,^{30,24} C. BIWER,⁶¹ M. A. BIZOUARD,²⁸
 874 J. K. BLACKBURN,¹ J. BLACKMAN,⁴⁷ C. D. BLAIR,^{1,66} D. G. BLAIR,⁶⁶ R. M. BLAIR,⁴⁶ S. BLOEMEN,⁶⁷ O. BOCK,¹⁰
 875 N. BODE,¹⁰ M. BOER,⁶⁸ G. BOGAERT,⁶⁸ A. BOHE,³⁸ F. BONDU,⁶⁹ E. BONILLA,⁵⁰ R. BONNAND,⁸ B. A. BOOM,¹⁴ R. BORK,¹
 876 V. BOSCHI,^{30,24} S. BOSE,^{70,19} K. BOSSIE,⁷ Y. BOUFFANAIS,³⁹ A. BOZZI,³⁰ C. BRADASCHIA,²⁴ P. R. BRADY,²¹
 877 M. BRANCHESI,^{17,18} J. E. BRAU,⁷¹ T. BRIANT,⁷² A. BRILLET,⁶⁸ M. BRINKMANN,¹⁰ V. BRISSON,²⁸ P. BROCKILL,²¹
 878 J. E. BROIDA,⁷³ A. F. BROOKS,¹ D. D. BROWN,⁷⁴ S. BRUNETT,¹ C. C. BUCHANAN,² A. BUIKEMA,¹⁵ T. BULIK,⁷⁵
 879 H. J. BULTEN,^{76,14} A. BUONANNO,^{38,77} D. BUSKULIC,⁸ C. BUY,³⁹ R. L. BYER,⁵⁰ M. CABERO,¹⁰ L. CADONATI,⁷⁸
 880 G. CAGNOLI,^{26,79} C. CAHILLANE,¹ J. CALDERÓN BUSTILLO,⁷⁸ T. A. CALLISTER,¹ E. CALLONI,^{80,4} J. B. CAMP,⁸¹
 881 M. CANEPA,^{82,60} P. CANIZARES,⁶⁷ K. C. CANNON,⁸³ H. CAO,⁷⁴ J. CAO,⁸⁴ C. D. CAPANO,¹⁰ E. CAPOCASA,³⁹
 882 F. CARBOGNANI,³⁰ S. CARIDE,⁸⁵ M. F. CARNEY,⁸⁶ J. CASANUEVA DIAZ,²⁸ C. CASENTINI,^{32,33} S. CAUDILL,^{21,14}
 883 M. CAVAGLIÀ,¹¹ F. CAVALIER,²⁸ R. CAVALIERI,³⁰ G. CELLA,²⁴ C. B. CEPEDA,¹ P. CERDÁ-DURÁN,⁸⁷ G. CERRETANI,^{23,24}
 884 E. CESARINI,^{88,33} S. J. CHAMBERLIN,⁶⁵ M. CHAN,⁴⁵ S. CHAO,⁸⁹ P. CHARLTON,⁹⁰ E. CHASE,⁹¹ E. CHASSANDE-MOTTIN,³⁹
 885 D. CHATTERJEE,²¹ B. D. CHEESEBORO,⁴¹ H. Y. CHEN,⁹² X. CHEN,⁶⁶ Y. CHEN,⁴⁷ H.-P. CHENG,⁵ H. CHIA,⁵
 886 A. CHINCARINI,⁶⁰ A. CHUMMO,³⁰ T. CHMIEL,⁸⁶ H. S. CHO,⁹³ M. CHO,⁷⁷ J. H. CHOW,²⁵ N. CHRISTENSEN,^{73,68} Q. CHU,⁶⁶
 887 A. J. K. CHUA,¹³ S. CHUA,⁷² A. K. W. CHUNG,⁹⁴ S. CHUNG,⁶⁶ G. CIANI,^{5,52,53} R. CIOLFI,^{95,96} C. E. CIRELLI,⁵⁰
 888 A. CIRONE,^{82,60} F. CLARA,⁴⁶ J. A. CLARK,⁷⁸ P. CLEARWATER,⁹⁷ F. CLEVA,⁶⁸ C. COCCHIERI,¹¹ E. COCCIA,^{17,18}
 889 P.-F. COHADON,⁷² D. COHEN,²⁸ A. COLLA,^{98,35} C. G. COLLETTE,⁹⁹ L. R. COMINSKY,¹⁰⁰ M. CONSTANCIO JR.,¹⁶ L. CONTI,⁵³
 890 S. J. COOPER,⁵⁹ P. CORBAN,⁷ T. R. CORBITT,² I. CORDERO-CARRIÓN,¹⁰¹ K. R. CORLEY,⁴⁹ A. CORSI,⁸⁵ S. CORTESE,³⁰
 891 C. A. COSTA,¹⁶ M. W. COUGHLIN,^{73,1} S. B. COUGHLIN,⁹¹ J.-P. COULON,⁶⁸ S. T. COUNTRYMAN,⁴⁹ P. COUVARES,¹
 892 P. B. COVAS,¹⁰² E. E. COWAN,⁷⁸ D. M. COWARD,⁶⁶ M. J. COWART,⁷ D. C. COYNE,¹ R. COYNE,⁸⁵ J. D. E. CREIGHTON,²¹
 893 T. D. CREIGHTON,¹⁰³ J. CRIFE,² S. G. CROWDER,¹⁰⁴ T. J. CULLEN,^{29,2} A. CUMMING,⁴⁵ L. CUNNINGHAM,⁴⁵ E. CUOCO,³⁰
 894 T. DAL CANTON,⁸¹ G. DÁLYA,⁵⁴ S. L. DANILISHIN,^{22,10} S. D'ANTONIO,³³ K. DANZMANN,^{22,10} A. DASGUPTA,¹⁰⁵
 895 C. F. DA SILVA COSTA,⁵ V. DATILO,³⁰ I. DAVE,⁶² M. DAVIER,²⁸ D. DAVIS,⁶¹ E. J. DAW,¹⁰⁶ B. DAY,⁷⁸ S. DE,⁶¹
 896 D. DEBRA,⁵⁰ J. DEGALLAIX,²⁶ M. DE LAURENTIS,^{17,4} S. DELÉGLISE,⁷² W. DEL POZZO,^{59,23,24} N. DEMOS,¹⁵ T. DENKER,¹⁰
 897 T. DENT,¹⁰ R. DE PIETRI,^{56,57} V. DERGACHEV,³⁸ R. DE ROSA,^{80,4} R. T. DE ROSA,⁷ C. DE ROSSI,^{26,30} R. DE SALVO,¹⁰⁷
 898 O. DE VARONA,¹⁰ J. DEVENSON,²⁷ S. DHURANDHAR,¹⁹ M. C. DÍAZ,¹⁰³ T. DIETRICH,³⁸ L. DI FIORE,⁴ M. DI GIOVANNI,^{108,96}
 899 T. DI GIROLAMO,^{49,80,4} A. DI LIETO,^{23,24} S. DI PACE,^{98,35} I. DI PALMA,^{98,35} F. DI RENZO,^{23,24} Z. DOCTOR,⁹²
 900 V. DOLIQUE,²⁶ F. DONOVAN,¹⁵ K. L. DOOLEY,¹¹ S. DORAVARI,¹⁰ I. DORRINGTON,³⁶ R. DOUGLAS,⁴⁵ M. DOVALE ÁLVAREZ,⁵⁹
 901 T. P. DOWNES,²¹ M. DRAGO,¹⁰ C. DREISSIGACKER,¹⁰ J. C. DRIGGERS,⁴⁶ Z. DU,⁸⁴ M. DUCROT,⁸ P. DUPEJ,⁴⁵
 902 S. E. DWYER,⁴⁶ T. B. EDO,¹⁰⁶ M. C. EDWARDS,⁷³ A. EFFLER,⁷ H.-B. EGGENSTEIN,^{38,10} P. EHRENS,¹ J. EICHHOLZ,¹
 903 S. S. EIKENBERRY,⁵ R. A. EISENSTEIN,¹⁵ R. C. ESSICK,¹⁵ D. ESTEVEZ,⁸ Z. B. ETIENNE,⁴¹ T. ETZEL,¹ M. EVANS,¹⁵
 904 T. M. EVANS,⁷ M. FACTOUROVICH,⁴⁹ V. FAFONE,^{32,33,17} H. FAIR,⁶¹ S. FAIRHURST,³⁶ X. FAN,⁸⁴ S. FARINON,⁶⁰ B. FARR,⁹²
 905 W. M. FARR,⁵⁹ E. J. FAUCHON-JONES,³⁶ M. FAVATA,¹⁰⁹ M. FAYS,³⁶ C. FEE,⁸⁶ H. FEHRMANN,¹⁰ J. FEICHT,¹
 906 M. M. FEJER,⁵⁰ A. FERNANDEZ-GALIANA,¹⁵ I. FERRANTE,^{23,24} E. C. FERREIRA,¹⁶ F. FERRINI,³⁰ F. FIDECARO,^{23,24}
 907 D. FINSTAD,⁶¹ I. FIORI,³⁰ D. FIORUCCI,³⁹ M. FISHBACH,⁹² R. P. FISHER,⁶¹ M. FITZ-AXEN,⁴⁴ R. FLAMINIO,^{26,110}
 908 M. FLETCHER,⁴⁵ E. FLYNN,²⁹ H. FONG,¹¹¹ J. A. FONT,^{87,112} P. W. F. FORSYTH,²⁵ S. S. FORSYTH,⁷⁸ J.-D. FOURNIER,⁶⁸
 909 S. FRASCA,^{98,35} F. FRASCONI,²⁴ Z. FREI,⁵⁴ A. FREISE,⁵⁹ R. FREY,⁷¹ V. FREY,²⁸ E. M. FRIES,¹ P. FRITSCHER,¹⁵
 910 V. V. FROLOV,⁷ P. FULDA,⁵ M. FYFFE,⁷ H. GABBARD,⁴⁵ B. U. GADRE,¹⁹ S. M. GAEBEL,⁵⁹ J. R. GAIR,¹¹³
 911 L. GAMMAITONI,⁴² M. R. GANIJA,⁷⁴ S. G. GAONKAR,¹⁹ C. GARCIA-QUIROS,¹⁰² F. GARUFI,^{80,4} B. GATELEY,⁴⁶ S. GAUDIO,³⁷
 912 G. GAUR,¹¹⁴ V. GAYATHRI,¹¹⁵ N. GEHRELS,^{81,*} G. GEMME,⁶⁰ E. GENIN,³⁰ A. GENNAI,²⁴ D. GEORGE,¹² J. GEORGE,⁶²
 913 L. GERGELY,¹¹⁶ V. GERMAIN,⁸ S. GHONGE,⁷⁸ ABHIRUP GHOSH,²⁰ ARCHISMAN GHOSH,^{20,14} S. GHOSH,^{67,14,21}
 914 J. A. GIAIME,^{2,7} K. D. GIARDINA,⁷ A. GIAZOTTO,²⁴ K. GILL,³⁷ L. GLOVER,¹⁰⁷ E. GOETZ,¹¹⁷ R. GOETZ,⁵ S. GOMES,³⁶
 915 B. GONCHAROV,⁶ G. GONZÁLEZ,² J. M. GONZALEZ CASTRO,^{23,24} A. GOPAKUMAR,¹¹⁸ M. L. GORODETSKY,⁶³
 916 S. E. GOSSAN,¹ M. GOSELIN,³⁰ R. GOUATY,⁸ A. GRADO,^{119,4} C. GRAEF,⁴⁵ M. GRANATA,²⁶ A. GRANT,⁴⁵ S. GRAS,¹⁵
 917 C. GRAY,⁴⁶ G. GRECO,^{120,121} A. C. GREEN,⁵⁹ E. M. GRETARSSON,³⁷ P. GROOT,⁶⁷ H. GROTE,¹⁰ S. GRUNEWALD,³⁸
 918 P. GRUNING,²⁸ G. M. GUIDI,^{120,121} X. GUO,⁸⁴ A. GUPTA,⁶⁵ M. K. GUPTA,¹⁰⁵ K. E. GUSHWA,¹ E. K. GUSTAFSON,¹

- 919 R. GUSTAFSON,¹¹⁷ O. HALIM,^{18,17} B. R. HALL,⁷⁰ E. D. HALL,¹⁵ E. Z. HAMILTON,³⁶ G. HAMMOND,⁴⁵ M. HANEY,¹²²
920 M. M. HANKE,¹⁰ J. HANKS,⁴⁶ C. HANNA,⁶⁵ M. D. HANNAM,³⁶ O. A. HANNUKSELA,⁹⁴ J. HANSON,⁷ T. HARDWICK,²
921 J. HARMS,^{17,18} G. M. HARRY,¹²³ I. W. HARRY,³⁸ M. J. HART,⁴⁵ C.-J. HASTER,¹¹¹ K. HAUGHIAN,⁴⁵ J. HEALY,⁵⁸
922 A. HEIDMANN,⁷² M. C. HEINTZE,⁷ H. HEITMANN,⁶⁸ P. HELLO,²⁸ G. HEMMING,³⁰ M. HENDRY,⁴⁵ I. S. HENG,⁴⁵ J. HENNIG,⁴⁵
923 A. W. HEPTONSTALL,¹ M. HEURS,^{10,22} S. HILD,⁴⁵ T. HINDERER,⁶⁷ D. HOAK,³⁰ D. HOFMAN,²⁶ K. HOLT,⁷ D. E. HOLZ,⁹²
924 P. HOPKINS,³⁶ C. HORST,²¹ J. HOUGH,⁴⁵ E. A. HOUSTON,⁴⁵ E. J. HOWELL,⁶⁶ A. HREIBI,⁶⁸ Y. M. HU,¹⁰ E. A. HUERTA,¹²
925 D. HUET,²⁸ B. HUGHEY,³⁷ S. HUSA,¹⁰² S. H. HUTTNER,⁴⁵ T. HUYNH-DINH,⁷ N. INDIK,¹⁰ R. INTA,⁸⁵ G. INTINI,^{98,35}
926 H. N. ISA,⁴⁵ J.-M. ISAC,⁷² M. ISI,¹ B. R. IYER,²⁰ K. IZUMI,⁴⁶ T. JACQMIN,⁷² K. JANI,⁷⁸ P. JARANOWSKI,¹²⁴ S. JAWAHAR,⁶⁴
927 F. JIMÉNEZ-FORTEZA,¹⁰² W. W. JOHNSON,² N. K. JOHNSON-MCDANIEL,¹³ D. I. JONES,¹²⁵ R. JONES,⁴⁵ R. J. G. JONKER,¹⁴
928 L. JU,⁶⁶ J. JUNKER,¹⁰ C. V. KALAGHATGI,³⁶ V. KALOGERA,⁹¹ B. KAMAI,¹ S. KANDHASAMY,⁷ G. KANG,⁴⁰ J. B. KANNER,¹
929 S. J. KAPADIA,²¹ S. KARKI,⁷¹ K. S. KARVINEN,¹⁰ M. KASPRZACK,² W. KASTAUN,¹⁰ M. KATOLIK,¹² E. KATSAVOUNIDIS,¹⁵
930 W. KATZMAN,⁷ S. KAUFER,²² K. KAWABE,⁴⁶ K. KAWAGUCHI,³⁸ F. KÉFÉLIAN,⁶⁸ D. KEITEL,⁴⁵ A. J. KEMBALL,¹²
931 R. KENNEDY,¹⁰⁶ C. KENT,³⁶ J. S. KEY,¹²⁶ F. Y. KHALILI,⁶³ I. KHAN,^{17,33} S. KHAN,¹⁰ Z. KHAN,¹⁰⁵ E. A. KHAZANOV,¹²⁷
932 N. KIJBUNCHOO,²⁵ CHUNGLEE KIM,¹²⁸ J. C. KIM,¹²⁹ K. KIM,⁹⁴ W. S. KIM,¹³⁰ Y.-M. KIM,⁹³ S. J. KIMBRELL,⁷⁸
933 E. J. KING,⁷⁴ P. J. KING,⁴⁶ M. KINLEY-HANLON,¹²³ R. KIRCHHOFF,¹⁰ J. S. KISSEL,⁴⁶ L. KLEYBOLTE,³⁴ S. KLIMENKO,⁵
934 T. D. KNOWLES,⁴¹ P. KOCH,¹⁰ S. M. KOEHLLENBECK,¹⁰ S. KOLEY,¹⁴ V. KONDRASHOV,¹ A. KONTOS,¹⁵ M. KOROBKO,³⁴
935 W. Z. KORTH,¹ I. KOWALSKA,⁷⁵ D. B. KOZAK,¹ C. KRÄMER,¹⁰ V. KRINGEL,¹⁰ B. KRISHNAN,¹⁰ A. KRÓLAK,^{131,132}
936 G. KUEHN,¹⁰ P. KUMAR,¹¹¹ R. KUMAR,¹⁰⁵ S. KUMAR,²⁰ L. KUO,⁸⁹ A. KUTYNIA,¹³¹ S. KWANG,²¹ B. D. LACKEY,³⁸
937 K. H. LAI,⁹⁴ M. LANDRY,⁴⁶ R. N. LANG,¹³³ J. LANGE,⁵⁸ B. LANTZ,⁵⁰ R. K. LANZA,¹⁵ A. LARTAUX-VOLLARD,²⁸
938 P. D. LASKY,⁶ M. LAXEN,⁷ A. LAZZARINI,¹ C. LAZZARO,⁵³ P. LEACI,^{98,35} S. LEAVEY,⁴⁵ C. H. LEE,⁹³ H. K. LEE,¹³⁴
939 H. M. LEE,¹³⁵ H. W. LEE,¹²⁹ K. LEE,⁴⁵ J. LEHMANN,¹⁰ A. LENON,⁴¹ M. LEONARDI,^{108,96} N. LEROY,²⁸ N. LETENDRE,⁸
940 Y. LEVIN,⁶ T. G. F. LI,⁹⁴ S. D. LINKER,¹⁰⁷ J. LIU,⁶⁶ X. LIU,²¹ R. K. L. LO,⁹⁴ N. A. LOCKERBIE,⁶⁴ L. T. LONDON,³⁶
941 J. E. LORD,⁶¹ M. LORENZINI,^{17,18} V. LORLETTE,¹³⁶ M. LORMAND,⁷ G. LOSURDO,²⁴ J. D. LOUGH,¹⁰ C. O. LOUSTO,⁵⁸
942 G. LOVELACE,²⁹ H. LÜCK,^{22,10} D. LUMACA,^{32,33} A. P. LUNDGREN,¹⁰ R. LYNCH,¹⁵ Y. MA,⁴⁷ R. MACAS,³⁶ S. MACFOY,²⁷
943 B. MACHENSCHALK,¹⁰ M. MACINNIS,¹⁵ D. M. MACLEOD,³⁶ I. MAGAÑA HERNANDEZ,²¹ F. MAGAÑA-SANDOVAL,⁶¹
944 L. MAGAÑA ZERTUCHE,⁶¹ R. M. MAGEE,⁶⁵ E. MAJORANA,³⁵ I. MAKSIMOVIC,¹³⁶ N. MAN,⁶⁸ V. MANDIC,⁴⁴ V. MANGANO,⁴⁵
945 G. L. MANSELL,²⁵ M. MANSKE,^{21,25} M. MANTOVANI,³⁰ F. MARCHESONI,^{51,43} F. MARION,⁸ S. MÁRKA,⁴⁹ Z. MÁRKA,⁴⁹
946 C. MARKAKIS,¹² A. S. MARKOSYAN,⁵⁰ A. MARKOWITZ,¹ E. MAROS,¹ A. MARQUINA,¹⁰¹ F. MARTELLI,^{120,121}
947 L. MARTELLINI,⁶⁸ I. W. MARTIN,⁴⁵ R. M. MARTIN,¹⁰⁹ D. V. MARTYNOV,¹⁵ K. MASON,¹⁵ E. MASSERA,¹⁰⁶ A. MASSEROT,⁸
948 T. J. MASSINGER,¹ M. MASSO-REID,⁴⁵ S. MASTROGIOVANNI,^{98,35} A. MATAS,⁴⁴ F. MATICHARD,^{1,15} L. MATONE,⁴⁹
949 N. MAVALVALA,¹⁵ N. MAZUMDER,⁷⁰ R. MCCARTHY,⁴⁶ D. E. MCCLELLAND,²⁵ S. MCCORMICK,⁷ L. MCCULLER,¹⁵
950 S. C. MCGUIRE,¹³⁷ G. MCINTYRE,¹ J. MCIVER,¹ D. J. MCMANUS,²⁵ L. MCNEILL,⁶ T. MCRAE,²⁵ S. T. MCWILLIAMS,⁴¹
951 D. MEACHER,⁶⁵ G. D. MEADORS,^{38,10} M. MEHMET,¹⁰ J. MEIDAM,¹⁴ E. MEJUTO-VILLA,⁹ A. MELATOS,⁹⁷ G. MENDELL,⁴⁶
952 R. A. MERCER,²¹ E. L. MERILH,⁴⁶ M. MERZOUGUI,⁶⁸ S. MESHKOV,¹ C. MESSENGER,⁴⁵ C. MESSICK,⁶⁵ R. METZDORFF,⁷²
953 P. M. MEYERS,⁴⁴ H. MIAO,⁵⁹ C. MICHEL,²⁶ H. MIDDLETON,⁵⁹ E. E. MIKHAILOV,¹³⁸ L. MILANO,^{80,4} A. L. MILLER,^{5,98,35}
954 B. B. MILLER,⁹¹ J. MILLER,¹⁵ M. C. MILOVICH-GOFF,¹⁰⁷ O. MINAZZOLI,^{68,139} Y. MINENKOV,³³ J. MING,³⁸ C. MISHRA,¹⁴⁰
955 S. MITRA,¹⁹ V. P. MITROFANOV,⁶³ G. MITSSELMAKHER,⁵ R. MITTLEMAN,¹⁵ D. MOFFA,⁸⁶ A. MOGGI,²⁴ K. MOGUSHI,¹¹
956 M. MOHAN,³⁰ S. R. P. MOHAPATRA,¹⁵ M. MONTANI,^{120,121} C. J. MOORE,¹³ D. MORARU,⁴⁶ G. MORENO,⁴⁶
957 S. R. MORRIS,¹⁰³ B. MOURS,⁸ C. M. MOW-LOWRY,⁵⁹ G. MUELLER,⁵ A. W. MUIR,³⁶ ARUNAVA MUKHERJEE,¹⁰
958 D. MUKHERJEE,²¹ S. MUKHERJEE,¹⁰³ N. MUKUND,¹⁹ A. MULLAVEY,⁷ J. MUNCH,⁷⁴ E. A. MUÑIZ,⁶¹ M. MURATORE,³⁷
959 P. G. MURRAY,⁴⁵ K. NAPIER,⁷⁸ I. NARDECCHIA,^{32,33} L. NATICCHIONI,^{98,35} R. K. NAYAK,¹⁴¹ J. NEILSON,¹⁰⁷
960 G. NELEMANS,^{67,14} T. J. N. NELSON,⁷ M. NERY,¹⁰ A. NEUNZERT,¹¹⁷ L. NEVIN,¹ J. M. NEWPORT,¹²³ G. NEWTON,^{45,†}
961 K. K. Y. NG,⁹⁴ T. T. NGUYEN,²⁵ D. NICHOLS,⁶⁷ A. B. NIELSEN,¹⁰ S. NISSANKE,^{67,14} A. NITZ,¹⁰ A. NOACK,¹⁰
962 F. NOCERA,³⁰ D. NOLTING,⁷ C. NORTH,³⁶ L. K. NUTTALL,³⁶ J. OBERLING,⁴⁶ G. D. O'DEA,¹⁰⁷ G. H. OGIN,¹⁴² J. J. OH,¹³⁰
963 S. H. OH,¹³⁰ F. OHME,¹⁰ M. A. OKADA,¹⁶ M. OLIVER,¹⁰² P. OPPERMAN,¹⁰ RICHARD J. ORAM,⁷ B. O'REILLY,⁷
964 R. ORMISTON,⁴⁴ L. F. ORTEGA,⁵ R. O'SHAUGHNESSY,⁵⁸ S. OSSOKINE,³⁸ D. J. OTTAWAY,⁷⁴ H. OVERMIER,⁷ B. J. OWEN,⁸⁵
965 A. E. PACE,⁶⁵ J. PAGE,¹⁴³ M. A. PAGE,⁶⁶ A. PAI,^{115,144} S. A. PAI,⁶² J. R. PALAMOS,⁷¹ O. PALASHOV,¹²⁷ C. PALOMBA,³⁵
966 A. PAL-SINGH,³⁴ HOWARD PAN,⁸⁹ HUANG-WEI PAN,⁸⁹ B. PANG,⁴⁷ P. T. H. PANG,⁹⁴ C. PANKOW,⁹¹ F. PANNARALE,³⁶
967 B. C. PANT,⁶² F. PAOLETTI,²⁴ A. PAOLI,³⁰ M. A. PAPA,^{38,21,10} A. PARIDA,¹⁹ W. PARKER,⁷ D. PASCUCCI,⁴⁵
968 A. PASQUALETTI,³⁰ R. PASSAQUIETI,^{23,24} D. PASSUELLO,²⁴ M. PATIL,¹³² B. PATRICELLI,^{145,24} B. L. PEARLSTONE,⁴⁵
969 M. PEDRAZA,¹ R. PEDURAND,^{26,146} L. PEKOWSKY,⁶¹ A. PELE,⁷ S. PENN,¹⁴⁷ C. J. PEREZ,⁴⁶ A. PERRECA,^{1,108,96}
970 L. M. PERRI,⁹¹ H. P. PFEIFFER,^{111,38} M. PHELPS,⁴⁵ K. PHUKON,⁷⁰ O. J. PICCINNI,^{98,35} M. PICHOT,⁶⁸
971 F. PIERGIOVANNI,^{120,121} V. PIERRO,⁹ G. PILLANT,³⁰ L. PINARD,²⁶ I. M. PINTO,⁹ M. PIRELLO,⁴⁶ M. PITKIN,⁴⁵ M. POE,²¹
972 R. POGGIANI,^{23,24} P. POPOLIZIO,³⁰ E. K. PORTER,³⁹ A. POST,¹⁰ J. POWELL,^{45,148} J. PRASAD,¹⁹ J. W. W. PRATT,³⁷
973 G. PRATTEN,¹⁰² V. PREDOI,³⁶ T. PRESTEGARD,²¹ M. PRIJATELJ,¹⁰ M. PRINCIPE,⁹ S. PRIVITERA,³⁸ G. A. PRODI,^{108,96}
974 L. G. PROKHOROV,⁶³ O. PUNCKEN,¹⁰ M. PUNTURO,⁴³ P. PUPPO,³⁵ M. PÜRNER,³⁸ H. QI,²¹ V. QUETSCHKE,¹⁰³
975 E. A. QUINTERO,¹ R. QUITZOW-JAMES,⁷¹ D. S. RABELING,²⁵ H. RADKINS,⁴⁶ P. RAFFAI,⁵⁴ S. RAJA,⁶² C. RAJAN,⁶²
976 B. RAJBHANDARI,⁸⁵ M. RAKHMANOV,¹⁰³ K. E. RAMIREZ,¹⁰³ A. RAMOS-BUADES,^{102,35} P. RAPAGNANI,^{98,35} V. RAYMOND,³⁸
977 M. RAZZANO,^{23,24} J. READ,²⁹ T. REGIMBAU,⁶⁸ L. REI,⁶⁰ S. REID,⁶⁴ D. H. REITZE,^{1,5} W. REN,¹² S. D. REYES,⁶¹

978 F. RICCI,^{98,35} P. M. RICKER,¹² S. RIEGER,¹⁰ K. RILES,¹¹⁷ M. RIZZO,⁵⁸ N. A. ROBERTSON,^{1,45} R. ROBIE,⁴⁵ F. ROBINET,²⁸
 979 A. ROCCHI,³³ L. ROLLAND,⁸ J. G. ROLLINS,¹ V. J. ROMA,⁷¹ R. ROMANO,^{3,4} C. L. ROMEL,⁴⁶ J. H. ROMIE,⁷
 980 D. ROSIŃSKA,^{149,55} M. P. ROSS,¹⁵⁰ S. ROWAN,⁴⁵ A. RÜDIGER,¹⁰ P. RUGGI,³⁰ G. RUTINS,²⁷ K. RYAN,⁴⁶ S. SACHDEV,¹
 981 T. SADECKI,⁴⁶ L. SADEGHIAN,²¹ M. SAKELLARIADOU,¹⁵¹ L. SALCONI,³⁰ M. SALEEM,¹¹⁵ F. SALEMI,¹⁰ A. SAMAJDAR,¹⁴¹
 982 L. SAMMUT,⁶ L. M. SAMPSON,⁹¹ E. J. SANCHEZ,¹ L. E. SANCHEZ,¹ N. SANCHIS-GUAL,⁸⁷ V. SANDBERG,⁴⁶ J. R. SANDERS,⁶¹
 983 N. SARIN,⁶ B. SASSOLAS,²⁶ B. S. SATHYAPRAKASH,^{65,36} O. SAUTER,¹¹⁷ R. L. SAVAGE,⁴⁶ A. SAWADSKY,³⁴ P. SCHALE,⁷¹
 984 M. SCHEEL,⁴⁷ J. SCHEUER,⁹¹ J. SCHMIDT,¹⁰ P. SCHMIDT,^{1,67} R. SCHNABEL,³⁴ R. M. S. SCHOFIELD,⁷¹ A. SCHÖNBECK,³⁴
 985 E. SCHREIBER,¹⁰ D. SCHUETTE,^{10,22} B. W. SCHULTE,¹⁰ B. F. SCHUTZ,^{36,10} S. G. SCHWALBE,³⁷ J. SCOTT,⁴⁵ S. M. SCOTT,²⁵
 986 E. SEIDEL,¹² D. SELERS,⁷ A. S. SENGUPTA,¹⁵² D. SENTENAC,³⁰ V. SEQUINO,^{32,33,17} A. SERGEEV,¹²⁷ D. A. SHADDOCK,²⁵
 987 T. J. SHAFFER,⁴⁶ A. A. SHAH,¹⁴³ M. S. SHAHRIAR,⁹¹ M. B. SHANER,¹⁰⁷ L. SHAO,³⁸ B. SHAPIRO,⁵⁰ P. SHAWHAN,⁷⁷
 988 A. SHEPERD,²¹ D. H. SHOEMAKER,¹⁵ D. M. SHOEMAKER,⁷⁸ K. SIELLEZ,⁷⁸ X. SIEMENS,²¹ M. SIENIAWSKA,⁵⁵ D. SIGG,⁴⁶
 989 A. D. SILVA,¹⁶ L. P. SINGER,⁸¹ A. SINGH,^{38,10,22} A. SINGHAL,^{17,35} A. M. SINTES,¹⁰² J. SK,⁷⁰ B. J. J. SLAGMOLEN,²⁵
 990 B. SMITH,⁷ J. R. SMITH,²⁹ R. J. E. SMITH,^{1,6} S. SOMALA,¹⁵³ E. J. SON,¹³⁰ J. A. SONNENBERG,²¹ B. SORAZU,⁴⁵
 991 F. SORRENTINO,⁶⁰ T. SOURADEEP,¹⁹ E. SOWELL,⁸⁵ A. P. SPENCER,⁴⁵ A. K. SRIVASTAVA,¹⁰⁵ K. STAATS,³⁷ A. STALEY,⁴⁹
 992 M. STEINKE,¹⁰ J. STEINLECHNER,^{34,45} S. STEINLECHNER,³⁴ D. STEINMEYER,¹⁰ S. P. STEVENSON,^{59,148} R. STONE,¹⁰³
 993 D. J. STOPS,⁵⁹ K. A. STRAIN,⁴⁵ G. STRATTA,^{120,121} S. E. STRIGIN,⁶³ A. STRUNK,⁴⁶ R. STURANI,¹⁵⁴ A. L. STUVER,⁷
 994 T. Z. SUMMERSCALES,¹⁵⁵ L. SUN,⁹⁷ S. SUNIL,¹⁰⁵ J. SURESH,¹⁹ P. J. SUTTON,³⁶ B. L. SWINKELS,³⁰ M. J. SZCZEPAŃCZYK,³⁷
 995 M. TACCA,¹⁴ S. C. TAIT,⁴⁵ C. TALBOT,⁶ D. TALUKDER,⁷¹ D. B. TANNER,⁵ M. TÁPAI,¹¹⁶ A. TARACCHINI,³⁸ J. D. TASSON,⁷³
 996 J. A. TAYLOR,¹⁴³ R. TAYLOR,¹ S. V. TEWARI,¹⁴⁷ T. THEEG,¹⁰ F. THIES,¹⁰ E. G. THOMAS,⁵⁹ M. THOMAS,⁷ P. THOMAS,⁴⁶
 997 K. A. THORNE,⁷ E. THRANE,⁶ S. TIWARI,^{17,96} V. TIWARI,³⁶ K. V. TOKMAKOV,⁶⁴ K. TOLAND,⁴⁵ M. TONELLI,^{23,24}
 998 Z. TORNASI,⁴⁵ A. TORRES-FORNÉ,⁸⁷ C. I. TORRIE,¹ D. TÖYRÄ,⁵⁹ F. TRAVASSO,^{30,43} G. TRAYLOR,⁷ J. TRINASTIC,⁵
 999 M. C. TRINGALI,^{108,96} L. TROZZO,^{156,24} K. W. TSANG,¹⁴ M. TSE,¹⁵ R. TSO,¹ L. TSUKADA,⁸³ D. TSUNA,⁸³
 1000 D. TUYENBAYEV,¹⁰³ K. UENO,²¹ D. UGOLINI,¹⁵⁷ C. S. UNNIKRIISHNAN,¹¹⁸ A. L. URBAN,¹ S. A. USMAN,³⁶ H. VAHLBRUCH,²²
 1001 G. VAJENTE,¹ G. VALDES,² N. VAN BAKEL,¹⁴ M. VAN BEUZEKOM,¹⁴ J. F. J. VAN DEN BRAND,^{76,14}
 1002 C. VAN DEN BROECK,^{14,158} D. C. VANDER-HYDE,⁶¹ L. VAN DER SCHAAF,¹⁴ J. V. VAN HEIJNINGEN,¹⁴ A. A. VAN VEGGEL,⁴⁵
 1003 M. VARDARO,^{52,53} V. VARMA,⁴⁷ S. VASS,¹ M. VASÚTH,⁴⁸ A. VECCHIO,⁵⁹ G. VEDOVATO,⁵³ J. VEITCH,⁴⁵ P. J. VEITCH,⁷⁴
 1004 K. VENKATESWARA,¹⁵⁰ G. VENUGOPALAN,¹ D. VERKINDT,⁸ F. VETRANO,^{120,121} A. VICERÉ,^{120,121} A. D. VIETS,²¹
 1005 S. VINCIGUERRA,⁵⁹ D. J. VINE,²⁷ J.-Y. VINET,⁶⁸ S. VITALE,¹⁵ T. VO,⁶¹ H. VOCCA,^{42,43} C. VORVICK,⁴⁶
 1006 S. P. VYATCHANIN,⁶³ A. R. WADE,¹ L. E. WADE,⁸⁶ M. WADE,⁸⁶ R. WALET,¹⁴ M. WALKER,²⁹ L. WALLACE,¹
 1007 S. WALSH,^{38,10,21} G. WANG,^{17,121} H. WANG,⁵⁹ J. Z. WANG,⁶⁵ W. H. WANG,¹⁰³ Y. F. WANG,⁹⁴ R. L. WARD,²⁵ J. WARNER,⁴⁶
 1008 M. WAS,⁸ J. WATCHI,⁹⁹ B. WEAVER,⁴⁶ L.-W. WEI,^{10,22} M. WEINERT,¹⁰ A. J. WEINSTEIN,¹ R. WEISS,¹⁵ L. WEN,⁶⁶
 1009 E. K. WESSEL,¹² P. WESSELS,¹⁰ J. WESTERWECK,¹⁰ T. WESTPHAL,¹⁰ K. WETTE,²⁵ J. T. WHELAN,⁵⁸ D. WHITE,²⁹
 1010 B. F. WHITING,⁵ C. WHITTLE,⁶ D. WILKEN,¹⁰ D. WILLIAMS,⁴⁵ R. D. WILLIAMS,¹ A. R. WILLIAMSON,⁶⁷ J. L. WILLIS,^{1,159}
 1011 B. WILLKE,^{22,10} M. H. WIMMER,¹⁰ W. WINKLER,¹⁰ C. C. WIPF,¹ H. WITTEL,^{10,22} G. WOAN,⁴⁵ J. WOEHLE,¹⁰
 1012 J. WOFFORD,⁵⁸ K. W. K. WONG,⁹⁴ J. WORDEN,⁴⁶ J. L. WRIGHT,⁴⁵ D. S. WU,¹⁰ D. M. WYSOCKI,⁵⁸ H. YAMAMOTO,¹
 1013 C. C. YANCEY,⁷⁷ L. YANG,¹⁶⁰ M. J. YAP,²⁵ M. YAZBACK,⁵ HANG YU,¹⁵ HAOCUN YU,¹⁵ M. YVERT,⁸ A. ZADROŻNY,¹³¹
 1014 M. ZANOLIN,³⁷ T. ZELENKOVA,³⁰ J.-P. ZENDRI,⁵³ M. ZEVIN,⁹¹ L. ZHANG,¹ M. ZHANG,¹³⁸ T. ZHANG,⁴⁵ Y.-H. ZHANG,⁵⁸
 1015 C. ZHAO,⁶⁶ M. ZHOU,⁹¹ Z. ZHOU,⁹¹ S. J. ZHU,^{38,10} X. J. ZHU,⁶ A. B. ZIMMERMAN,¹¹¹ M. E. ZUCKER,^{1,15} AND J. ZWEIZIG¹
 1016 LIGO SCIENTIFIC COLLABORATION AND VIRGO COLLABORATION

1017 ¹ *LIGO, California Institute of Technology, Pasadena, CA 91125, USA*

1018 ² *Louisiana State University, Baton Rouge, LA 70803, USA*

1019 ³ *Università di Salerno, Fisciano, I-84084 Salerno, Italy*

1020 ⁴ *INFN, Sezione di Napoli, Complesso Universitario di Monte S. Angelo, I-80126 Napoli, Italy*

1021 ⁵ *University of Florida, Gainesville, FL 32611, USA*

1022 ⁶ *OzGrav, School of Physics & Astronomy, Monash University, Clayton 3800, Victoria, Australia*

1023 ⁷ *LIGO Livingston Observatory, Livingston, LA 70754, USA*

1024 ⁸ *Laboratoire d'Annecy-le-Vieux de Physique des Particules (LAPP), Université Savoie Mont Blanc, CNRS/IN2P3, F-74941 Annecy, France*

1026 ⁹ *University of Sannio at Benevento, I-82100 Benevento, Italy and INFN, Sezione di Napoli, I-80100 Napoli, Italy*

1027 ¹⁰ *Max Planck Institute for Gravitational Physics (Albert Einstein Institute), D-30167 Hannover, Germany*

1028 ¹¹ *The University of Mississippi, University, MS 38677, USA*

1029 ¹² *NCSA, University of Illinois at Urbana-Champaign, Urbana, IL 61801, USA*

1030 ¹³ *University of Cambridge, Cambridge CB2 1TN, United Kingdom*

1031 ¹⁴ *Nikhef, Science Park, 1098 XG Amsterdam, The Netherlands*

- 1032 ¹⁵ *LIGO, Massachusetts Institute of Technology, Cambridge, MA 02139, USA*
- 1033 ¹⁶ *Instituto Nacional de Pesquisas Espaciais, 12227-010 São José dos Campos, São Paulo, Brazil*
- 1034 ¹⁷ *Gran Sasso Science Institute (GSSI), I-67100 L'Aquila, Italy*
- 1035 ¹⁸ *INFN, Laboratori Nazionali del Gran Sasso, I-67100 Assergi, Italy*
- 1036 ¹⁹ *Inter-University Centre for Astronomy and Astrophysics, Pune 411007, India*
- 1037 ²⁰ *International Centre for Theoretical Sciences, Tata Institute of Fundamental Research, Bengaluru 560089, India*
- 1038 ²¹ *University of Wisconsin-Milwaukee, Milwaukee, WI 53201, USA*
- 1039 ²² *Leibniz Universität Hannover, D-30167 Hannover, Germany*
- 1040 ²³ *Università di Pisa, I-56127 Pisa, Italy*
- 1041 ²⁴ *INFN, Sezione di Pisa, I-56127 Pisa, Italy*
- 1042 ²⁵ *OzGrav, Australian National University, Canberra, Australian Capital Territory 0200, Australia*
- 1043 ²⁶ *Laboratoire des Matériaux Avancés (LMA), CNRS/IN2P3, F-69622 Villeurbanne, France*
- 1044 ²⁷ *SUPA, University of the West of Scotland, Paisley PA1 2BE, United Kingdom*
- 1045 ²⁸ *LAL, Univ. Paris-Sud, CNRS/IN2P3, Université Paris-Saclay, F-91898 Orsay, France*
- 1046 ²⁹ *California State University Fullerton, Fullerton, CA 92831, USA*
- 1047 ³⁰ *European Gravitational Observatory (EGO), I-56021 Cascina, Pisa, Italy*
- 1048 ³¹ *Chennai Mathematical Institute, Chennai 603103, India*
- 1049 ³² *Università di Roma Tor Vergata, I-00133 Roma, Italy*
- 1050 ³³ *INFN, Sezione di Roma Tor Vergata, I-00133 Roma, Italy*
- 1051 ³⁴ *Universität Hamburg, D-22761 Hamburg, Germany*
- 1052 ³⁵ *INFN, Sezione di Roma, I-00185 Roma, Italy*
- 1053 ³⁶ *Cardiff University, Cardiff CF24 3AA, United Kingdom*
- 1054 ³⁷ *Embry-Riddle Aeronautical University, Prescott, AZ 86301, USA*
- 1055 ³⁸ *Max Planck Institute for Gravitational Physics (Albert Einstein Institute), D-14476 Potsdam-Golm, Germany*
- 1056 ³⁹ *APC, AstroParticule et Cosmologie, Université Paris Diderot, CNRS/IN2P3, CEA/Irfu, Observatoire de Paris, Sorbonne Paris Cité, F-75205 Paris Cedex 13, France*
- 1058 ⁴⁰ *Korea Institute of Science and Technology Information, Daejeon 34141, Korea*
- 1059 ⁴¹ *West Virginia University, Morgantown, WV 26506, USA*
- 1060 ⁴² *Università di Perugia, I-06123 Perugia, Italy*
- 1061 ⁴³ *INFN, Sezione di Perugia, I-06123 Perugia, Italy*
- 1062 ⁴⁴ *University of Minnesota, Minneapolis, MN 55455, USA*
- 1063 ⁴⁵ *SUPA, University of Glasgow, Glasgow G12 8QQ, United Kingdom*
- 1064 ⁴⁶ *LIGO Hanford Observatory, Richland, WA 99352, USA*
- 1065 ⁴⁷ *Caltech CaRT, Pasadena, CA 91125, USA*
- 1066 ⁴⁸ *Wigner RCP, RMKI, H-1121 Budapest, Konkoly Thege Miklós út 29-33, Hungary*
- 1067 ⁴⁹ *Columbia University, New York, NY 10027, USA*
- 1068 ⁵⁰ *Stanford University, Stanford, CA 94305, USA*
- 1069 ⁵¹ *Università di Camerino, Dipartimento di Fisica, I-62032 Camerino, Italy*
- 1070 ⁵² *Università di Padova, Dipartimento di Fisica e Astronomia, I-35131 Padova, Italy*
- 1071 ⁵³ *INFN, Sezione di Padova, I-35131 Padova, Italy*
- 1072 ⁵⁴ *Institute of Physics, Eötvös University, Pázmány P. s. 1/A, Budapest 1117, Hungary*
- 1073 ⁵⁵ *Nicolaus Copernicus Astronomical Center, Polish Academy of Sciences, 00-716, Warsaw, Poland*
- 1074 ⁵⁶ *Dipartimento di Scienze Matematiche, Fisiche e Informatiche, Università di Parma, I-43124 Parma, Italy*
- 1075 ⁵⁷ *INFN, Sezione di Milano Bicocca, Gruppo Collegato di Parma, I-43124 Parma, Italy*
- 1076 ⁵⁸ *Rochester Institute of Technology, Rochester, NY 14623, USA*
- 1077 ⁵⁹ *University of Birmingham, Birmingham B15 2TT, United Kingdom*
- 1078 ⁶⁰ *INFN, Sezione di Genova, I-16146 Genova, Italy*
- 1079 ⁶¹ *Syracuse University, Syracuse, NY 13244, USA*
- 1080 ⁶² *RRCAT, Indore MP 452013, India*
- 1081 ⁶³ *Faculty of Physics, Lomonosov Moscow State University, Moscow 119991, Russia*
- 1082 ⁶⁴ *SUPA, University of Strathclyde, Glasgow G1 1XQ, United Kingdom*
- 1083 ⁶⁵ *The Pennsylvania State University, University Park, PA 16802, USA*
- 1084 ⁶⁶ *OzGrav, University of Western Australia, Crawley, Western Australia 6009, Australia*
- 1085 ⁶⁷ *Department of Astrophysics/IMAPP, Radboud University Nijmegen, P.O. Box 9010, 6500 GL Nijmegen, The Netherlands*

- 1086 ⁶⁸ *Artemis, Université Côte d'Azur, Observatoire Côte d'Azur, CNRS, CS 34229, F-06304 Nice Cedex 4, France*
- 1087 ⁶⁹ *Institut FOTON, CNRS, Université de Rennes 1, F-35042 Rennes, France*
- 1088 ⁷⁰ *Washington State University, Pullman, WA 99164, USA*
- 1089 ⁷¹ *University of Oregon, Eugene, OR 97403, USA*
- 1090 ⁷² *Laboratoire Kastler Brossel, UPMC-Sorbonne Universités, CNRS, ENS-PSL Research University, Collège de France, F-75005 Paris,*
- 1091 *France*
- 1092 ⁷³ *Carleton College, Northfield, MN 55057, USA*
- 1093 ⁷⁴ *OzGrav, University of Adelaide, Adelaide, South Australia 5005, Australia*
- 1094 ⁷⁵ *Astronomical Observatory Warsaw University, 00-478 Warsaw, Poland*
- 1095 ⁷⁶ *VU University Amsterdam, 1081 HV Amsterdam, The Netherlands*
- 1096 ⁷⁷ *University of Maryland, College Park, MD 20742, USA*
- 1097 ⁷⁸ *Center for Relativistic Astrophysics, Georgia Institute of Technology, Atlanta, GA 30332, USA*
- 1098 ⁷⁹ *Université Claude Bernard Lyon 1, F-69622 Villeurbanne, France*
- 1099 ⁸⁰ *Università di Napoli 'Federico II,' Complesso Universitario di Monte S. Angelo, I-80126 Napoli, Italy*
- 1100 ⁸¹ *NASA Goddard Space Flight Center, Greenbelt, MD 20771, USA*
- 1101 ⁸² *Dipartimento di Fisica, Università degli Studi di Genova, I-16146 Genova, Italy*
- 1102 ⁸³ *RESCEU, University of Tokyo, Tokyo, 113-0033, Japan.*
- 1103 ⁸⁴ *Tsinghua University, Beijing 100084, China*
- 1104 ⁸⁵ *Texas Tech University, Lubbock, TX 79409, USA*
- 1105 ⁸⁶ *Kenyon College, Gambier, OH 43022, USA*
- 1106 ⁸⁷ *Departamento de Astronomía y Astrofísica, Universitat de València, E-46100 Burjassot, València, Spain*
- 1107 ⁸⁸ *Museo Storico della Fisica e Centro Studi e Ricerche Enrico Fermi, I-00184 Roma, Italy*
- 1108 ⁸⁹ *National Tsing Hua University, Hsinchu City, 30013 Taiwan, Republic of China*
- 1109 ⁹⁰ *Charles Sturt University, Wagga Wagga, New South Wales 2678, Australia*
- 1110 ⁹¹ *Center for Interdisciplinary Exploration & Research in Astrophysics (CIERA), Northwestern University, Evanston, IL 60208, USA*
- 1111 ⁹² *University of Chicago, Chicago, IL 60637, USA*
- 1112 ⁹³ *Pusan National University, Busan 46241, Korea*
- 1113 ⁹⁴ *The Chinese University of Hong Kong, Shatin, NT, Hong Kong*
- 1114 ⁹⁵ *INAF, Osservatorio Astronomico di Padova, I-35122 Padova, Italy*
- 1115 ⁹⁶ *INFN, Trento Institute for Fundamental Physics and Applications, I-38123 Povo, Trento, Italy*
- 1116 ⁹⁷ *OzGrav, University of Melbourne, Parkville, Victoria 3010, Australia*
- 1117 ⁹⁸ *Università di Roma 'La Sapienza,' I-00185 Roma, Italy*
- 1118 ⁹⁹ *Université Libre de Bruxelles, Brussels 1050, Belgium*
- 1119 ¹⁰⁰ *Sonoma State University, Rohnert Park, CA 94928, USA*
- 1120 ¹⁰¹ *Departamento de Matemáticas, Universitat de València, E-46100 Burjassot, València, Spain*
- 1121 ¹⁰² *Universitat de les Illes Balears, IAC3—IEEC, E-07122 Palma de Mallorca, Spain*
- 1122 ¹⁰³ *The University of Texas Rio Grande Valley, Brownsville, TX 78520, USA*
- 1123 ¹⁰⁴ *Bellevue College, Bellevue, WA 98007, USA*
- 1124 ¹⁰⁵ *Institute for Plasma Research, Bhat, Gandhinagar 382428, India*
- 1125 ¹⁰⁶ *The University of Sheffield, Sheffield S10 2TN, United Kingdom*
- 1126 ¹⁰⁷ *California State University, Los Angeles, 5151 State University Dr, Los Angeles, CA 90032, USA*
- 1127 ¹⁰⁸ *Università di Trento, Dipartimento di Fisica, I-38123 Povo, Trento, Italy*
- 1128 ¹⁰⁹ *Montclair State University, Montclair, NJ 07043, USA*
- 1129 ¹¹⁰ *National Astronomical Observatory of Japan, 2-21-1 Osawa, Mitaka, Tokyo 181-8588, Japan*
- 1130 ¹¹¹ *Canadian Institute for Theoretical Astrophysics, University of Toronto, Toronto, Ontario M5S 3H8, Canada*
- 1131 ¹¹² *Osservatori Astronomic, Universitat de València, E-46980 Paterna, València, Spain*
- 1132 ¹¹³ *School of Mathematics, University of Edinburgh, Edinburgh EH9 3FD, United Kingdom*
- 1133 ¹¹⁴ *University and Institute of Advanced Research, Koba Institutional Area, Gandhinagar Gujarat 382007, India*
- 1134 ¹¹⁵ *IISER-TVM, CET Campus, Trivandrum Kerala 695016, India*
- 1135 ¹¹⁶ *University of Szeged, Dóm tér 9, Szeged 6720, Hungary*
- 1136 ¹¹⁷ *University of Michigan, Ann Arbor, MI 48109, USA*
- 1137 ¹¹⁸ *Tata Institute of Fundamental Research, Mumbai 400005, India*
- 1138 ¹¹⁹ *INAF, Osservatorio Astronomico di Capodimonte, I-80131, Napoli, Italy*
- 1139 ¹²⁰ *Università degli Studi di Urbino 'Carlo Bo,' I-61029 Urbino, Italy*

- 1140 ¹²¹ *INFN, Sezione di Firenze, I-50019 Sesto Fiorentino, Firenze, Italy*
- 1141 ¹²² *Physik-Institut, University of Zurich, Winterthurerstrasse 190, 8057 Zurich, Switzerland*
- 1142 ¹²³ *American University, Washington, D.C. 20016, USA*
- 1143 ¹²⁴ *University of Białystok, 15-424 Białystok, Poland*
- 1144 ¹²⁵ *University of Southampton, Southampton SO17 1BJ, United Kingdom*
- 1145 ¹²⁶ *University of Washington Bothell, 18115 Campus Way NE, Bothell, WA 98011, USA*
- 1146 ¹²⁷ *Institute of Applied Physics, Nizhny Novgorod, 603950, Russia*
- 1147 ¹²⁸ *Korea Astronomy and Space Science Institute, Daejeon 34055, Korea*
- 1148 ¹²⁹ *Inje University Gimhae, South Gyeongsang 50834, Korea*
- 1149 ¹³⁰ *National Institute for Mathematical Sciences, Daejeon 34047, Korea*
- 1150 ¹³¹ *NCBJ, 05-400 Świerk-Otwock, Poland*
- 1151 ¹³² *Institute of Mathematics, Polish Academy of Sciences, 00656 Warsaw, Poland*
- 1152 ¹³³ *Hillsdale College, Hillsdale, MI 49242, USA*
- 1153 ¹³⁴ *Hanyang University, Seoul 04763, Korea*
- 1154 ¹³⁵ *Seoul National University, Seoul 08826, Korea*
- 1155 ¹³⁶ *ESPCI, CNRS, F-75005 Paris, France*
- 1156 ¹³⁷ *Southern University and A&M College, Baton Rouge, LA 70813, USA*
- 1157 ¹³⁸ *College of William and Mary, Williamsburg, VA 23187, USA*
- 1158 ¹³⁹ *Centre Scientifique de Monaco, 8 quai Antoine 1er, MC-98000, Monaco*
- 1159 ¹⁴⁰ *Indian Institute of Technology Madras, Chennai 600036, India*
- 1160 ¹⁴¹ *IISER-Kolkata, Mohanpur, West Bengal 741252, India*
- 1161 ¹⁴² *Whitman College, 345 Boyer Avenue, Walla Walla, WA 99362 USA*
- 1162 ¹⁴³ *NASA Marshall Space Flight Center, Huntsville, AL 35811, USA*
- 1163 ¹⁴⁴ *Indian Institute of Technology Bombay, Powai, Mumbai, Maharashtra 400076, India*
- 1164 ¹⁴⁵ *Scuola Normale Superiore, Piazza dei Cavalieri 7, I-56126 Pisa, Italy*
- 1165 ¹⁴⁶ *Université de Lyon, F-69361 Lyon, France*
- 1166 ¹⁴⁷ *Hobart and William Smith Colleges, Geneva, NY 14456, USA*
- 1167 ¹⁴⁸ *OzGrav, Swinburne University of Technology, Hawthorn VIC 3122, Australia*
- 1168 ¹⁴⁹ *Janusz Gil Institute of Astronomy, University of Zielona Góra, 65-265 Zielona Góra, Poland*
- 1169 ¹⁵⁰ *University of Washington, Seattle, WA 98195, USA*
- 1170 ¹⁵¹ *King's College London, University of London, London WC2R 2LS, United Kingdom*
- 1171 ¹⁵² *Indian Institute of Technology, Gandhinagar Ahmedabad Gujarat 382424, India*
- 1172 ¹⁵³ *Indian Institute of Technology Hyderabad, Sangareddy, Khandi, Telangana 502285, India*
- 1173 ¹⁵⁴ *International Institute of Physics, Universidade Federal do Rio Grande do Norte, Natal RN 59078-970, Brazil*
- 1174 ¹⁵⁵ *Andrews University, Berrien Springs, MI 49104, USA*
- 1175 ¹⁵⁶ *Università di Siena, I-53100 Siena, Italy*
- 1176 ¹⁵⁷ *Trinity University, San Antonio, TX 78212, USA*
- 1177 ¹⁵⁸ *Van Swinderen Institute for Particle Physics and Gravity, University of Groningen, Nijenborgh 4, 9747 AG Groningen, The Netherlands*
- 1178 ¹⁵⁹ *Abilene Christian University, Abilene, TX 79699, USA*
- 1179 ¹⁶⁰ *Colorado State University, Fort Collins, CO 80523, USA*

* Deceased, February 2017.

† Deceased, December 2016.